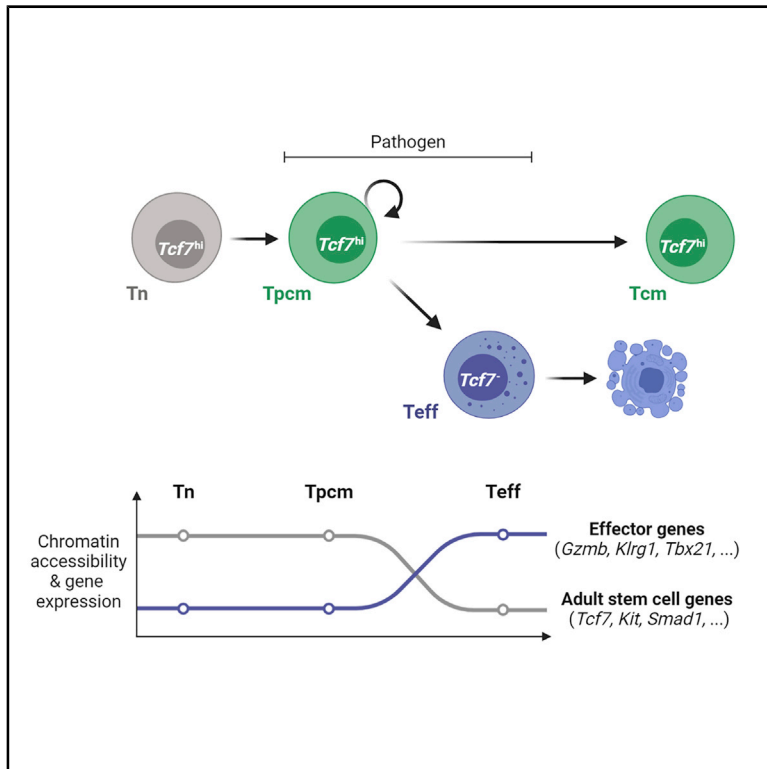# Central memory CD8⁺ T cells derive from stem-like *Tcf7*^hi effector cells in the absence of cytotoxic differentiation

Graphical Abstract

Authors

Daniela Pais Ferreira,
Joana Gomes Silva, Tania Wyss, ...,
Sanjiv A. Luther, Daniel E. Speiser,
Werner Held

Correspondence

werner.held@unil.ch

In Brief

Central memory is thought to emerge following pathogen clearance and to form based on de-differentiation of cytolytic effectors. Pais Ferreira et al. uncover rare effector-phase *Tcf7*^hi CD8⁺ T cells that do not pass through a cytotoxic effector differentiation state, already have central memory functions, and quantitatively yield central memory cells.

Highlights

- Effector-phase *Tcf7*^hi CD8⁺ T cells lack evidence of cytolytic differentiation

- Effector-phase *Tcf7*^hi cells quantitatively yield central memory cells

- *Tcf7*^hi cells have key properties of central memory cells, including stemness

- Tcf1 (*Tcf7*) ensures stemness by maintaining the expression of adult stem cell genes

CellPress

Article

Central memory CD8^{+} T cells derive from stem-like *Tcf7*^{hi} effector cells in the absence of cytotoxic differentiation

Daniela Pais Ferreira,[1] Joana Gomes Silva,[1] Tania Wyss,[2] Silvia A. Fuertes Marraco,[1] Léonardo Scarpellino,[3] Mélanie Charmoy,[1] Roeltje Maas,[1,4,5] Imran Siddiqui,[1] Li Tang,[6] Johanna A. Joyce,[1,4] Mauro Delorenzi,[1,2] Sanjiv A. Luther,[3] Daniel E. Speiser,[1] and Werner Held[1,7,*]

[1]Department of Oncology, University of Lausanne, 1066 Epalinges, Switzerland
[2]SIB Swiss Institute of Bioinformatics, Bioinformatics Core Facility, 1015 Lausanne, Switzerland
[3]Department of Biochemistry, University of Lausanne, 1066 Epalinges, Switzerland
[4]Ludwig Institute for Cancer Research, University of Lausanne, Lausanne, Switzerland
[5]Department of Neuroscience (Neuroscience Research Center), Centre Hospitalier Universitaire Vaudois, Lausanne, Switzerland
[6]Institute of Bioengineering, École polytechnique fédérale de Lausanne, Lausanne, 1015, Switzerland
[7]Lead Contact
*Correspondence: werner.held@unil.ch
https://doi.org/10.1016/j.immuni.2020.09.005

SUMMARY

Central memory CD8^{+} T cells (Tcm) control systemic secondary infections and can protect from chronic infection and cancer as a result of their stem-cell-like capacity to expand, differentiate, and self-renew. Central memory is generally thought to emerge following pathogen clearance and to form based on the de-differentiation of cytolytic effector cells. Here, we uncovered rare effector-phase CD8^{+} T cells expressing high amounts of the transcription factor *Tcf7* (Tcf1) that showed no evidence of prior cytolytic differentiation and that displayed key hallmarks of Tcm cells. These effector-phase *Tcf7*^{hi} cells quantitatively yielded Tcm cells based on lineage tracing. Mechanistically, Tcf1 counteracted the differentiation of *Tcf7*^{hi} cells and sustained the expression of conserved adult stem-cell genes that were critical for CD8^{+} T cell stemness. The discovery of stem-cell-like CD8^{+} T cells during the effector response to acute infection provides an opportunity to optimize Tcm cell formation by vaccination.

INTRODUCTION

Infection activates very rare antigen-specific naive CD8^{+} T cells (Tn), which expand and differentiate into cytotoxic effector cells (Teff) that clear pathogen-infected cells. While most antigen-specific cells die following pathogen clearance, some cells survive to form a diverse and long-lived memory compartment that protects against secondary infection. The potent protective capacity of central memory CD8^{+} T cells (Tcm) depends on their stem-cell-like properties to efficiently expand, differentiate into Teff cells, and self-renew (Graef et al., 2014). Since Tcm cells provide sustained secondary responses that have the potential to control chronic infections and cancer (Cui et al., 2009; Klebanoff et al., 2005; West et al., 2011), their generation is a central goal of vaccination. However, despite their importance, the molecular programs required for Tcm cell generation and maintenance are incompletely understood, which is related to the fact that the developmental origin of Tcm cells is still not fully resolved.

Several CD8^{+} T cell lineage relationship models explain the predominance of effector CD8^{+} T cells during an acute response and the emergence of memory cells after antigen clearance (Henning et al., 2018; Kaech and Cui, 2012). One model suggests

that Tn cells differentiate into Teff cells (acquire cytotoxic capacity), and occasional cells de-differentiate into Tcm cells (lose cytotoxic capacity) once the infection is cleared (Bannard et al., 2009; Youngblood et al., 2017). De-differentiation is not random, as certain effector populations are biased toward a memory fate (Chang et al., 2007; Joshi et al., 2007; Kakaradov et al., 2017). Such memory precursor (MP) cells nonetheless pass through a cytotoxic effector state, as judged by Granzyme B expression and cytotoxic activity (Joshi et al., 2007), and are thus also thought to de-differentiate in order to become Tcm cells. However, since most MP cells disappear during contraction (Kaech and Cui, 2012), it remains possible that memory derives from a specific subset of MP cells whose properties may or may not support this model. An alternative explanation is that Tn cells give rise to cells that have central memory function and that such cells yield Tcm cells and, upon further stimulation, Teff cells (Pace et al., 2018; Restifo and Gattinoni, 2013). However, to our knowledge, effector-phase CD8^{+} T cells that respond to infection and that have central memory function have not been identified.

The formation and function of Tcm cells depends on transcription factors like Tcf1 (*Tcf7*) (Jeannet et al., 2010; Zhao et al.,
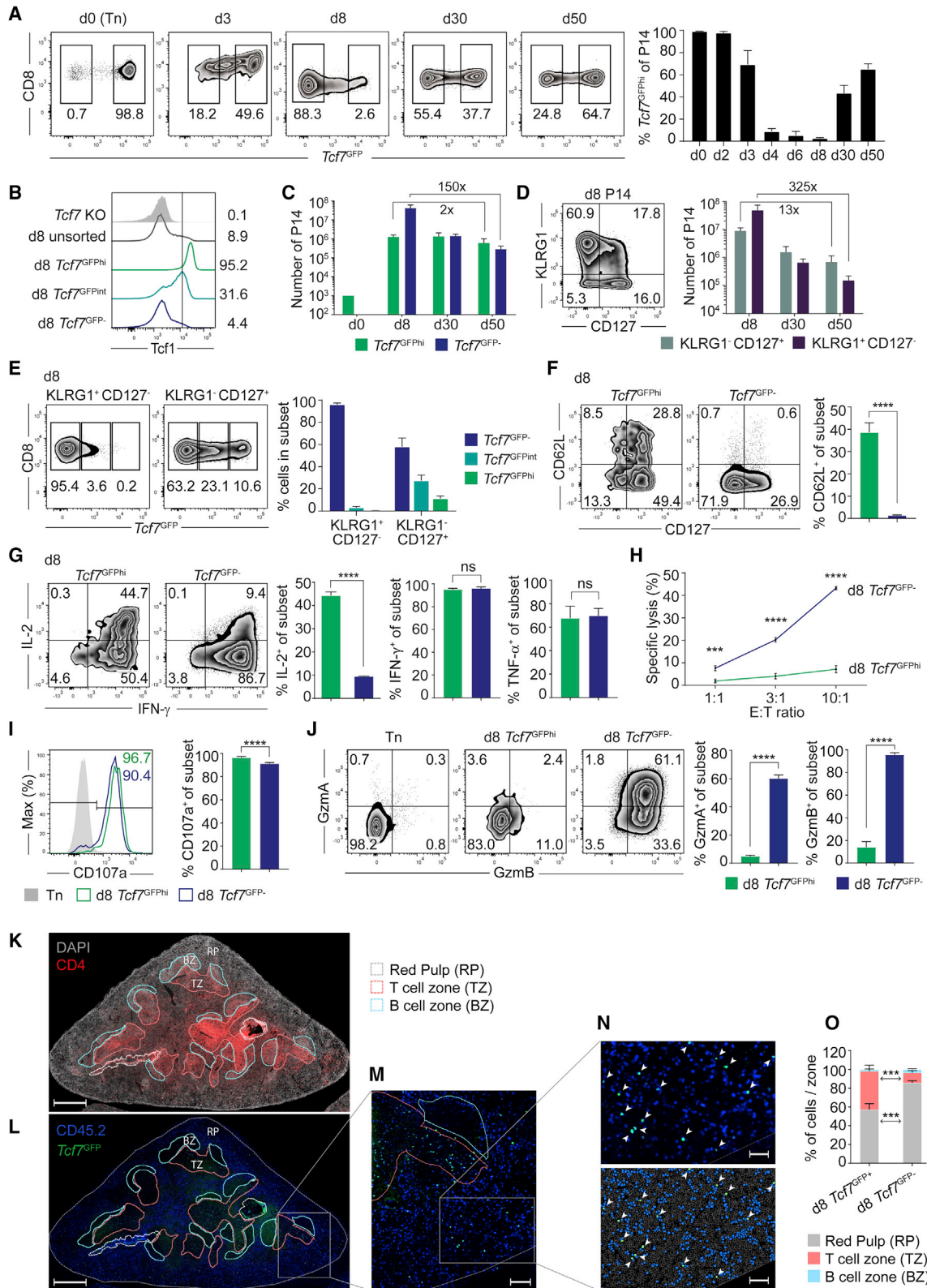
Figure 1. Effector-Stage *Tcf7*^hi CD8^+ T Cells Resemble Central Memory Cells

B6 (CD45.1/2) mice were adoptively transferred with *Tcf7*^GFP P14 cells (CD45.2) and infected with LCMV WE.

(A) *Tcf7*^GFP expression by splenic P14 cells at the indicated time points post-infection (p.i.).

2010), Id3 (Ji et al., 2011), STAT3 (Cui et al., 2011), Foxo1 (Hess Michelini et al., 2013; Kim et al., 2013), and c-Myb (Gautam et al., 2019). Absence of these factors reduces stemness and increases effector differentiation. Indeed, full effector differentiation is associated with epigenetic silencing of central memory genes (Gray et al., 2017; Ladle et al., 2016; Pace et al., 2018), suggesting that inhibition of effector differentiation is needed to maintain stemness. However, despite the availability of CD8+ stemness gene signatures (e.g., Pace et al., 2018), the functional relevance of such CD8+ T cell stemness programs has not been verified. The latter depends on the identification of effector-stage CD8+ T cells that have stem-cell properties or that quantitatively acquire stemness subsequent to pathogen clearance.

To address these questions, we followed the expression of the transcription factor Tcf1 (*Tcf7*), which plays a critical role for central memory formation (Jeannet et al., 2010; Zhao et al., 2010), during an acute CD8+ T cell response to viral infection. We found that high amounts of *Tcf7* expression defined a small subset of effector-phase CD8+ T cells that lacked cytolytic activity and that already had central memory properties, which relied on a set of Tcf1-dependent adult stem-cell genes. Central memory thus derives from stem-cell-like cells that are present during the effector response.

RESULTS

Tcf7 Expression Identifies Rare Effector-Phase CD8+ T Cells That Resemble Tcm Cells

To track the development of Tcm cells, we determined the expression of the transcription factor Tcf1 (*Tcf7*) in CD8+ T cells responding to acute viral infection. To this end, C57BL/6 (B6) recipient mice were transplanted with naive P14 CD8+ T cells (specific for the lymphocytic choriomeningitis virus [LCMV] gp33 epitope) expressing a *Tcf7*^{GFP} reporter one day before infection with LCMV WE strain, which causes acute resolved infection.

While naive *Tcf7*^{GFP} P14 cells highly expressed *Tcf7*^{GFP} (*Tcf7*^{GFPhi}), only 40%–60% of memory P14 cells were *Tcf7*^{GFPhi} (Figure 1A). The expression of *Tcf7*^{GFP} versus the classical central memory marker CD62L distinguished 3 main populations of memory cells (Figure S1A), which we analyzed separately for Tcm and effector memory (Tem) properties. These experiments revealed that *Tcf7*^{GFPhi} CD62L+ and *Tcf7*^{GFPhi} CD62L−, but not *Tcf7*$^{GFP-}$ CD62L− memory cells, had lymph-node homing capacity (Figure S1A), efficiently produced IL-2 (Figure S1B), and had increased recall expansion capacity (Figure S1C). Conversely,

Tcf7^{GFP-} CD62L− memory cells displayed hallmarks of Tem cells including increased expression of Granzyme A (GzmA), GzmB (Figure S1D), KLRG1, and the chemokine receptor CX3CR1 and reduced expression of CD127, as compared to *Tcf7*^{GFPhi} memory cells (Figure S1E). Despite subtle differences between CD62L+ and CD62L− *Tcf7*^{GFPhi} memory cells, these had Tcm properties, while CD62L− *Tcf7*$^{GFP-}$ cells qualified as Tem cells. Thus, CD62L− memory cells were heterogenous and included both Tcm and Tem cells.

We next followed *Tcf7*^{GFP} expression during the primary response to LCMV infection. Downregulation of *Tcf7*^{GFP} was observed in a subset of P14 cells starting on day 3 post-infection (d3 p.i.). By d4, most P14 cells were *Tcf7*$^{GFP-}$, and by d8, only 2%–3% remained *Tcf7*^{GFPhi} (Figure 1A). Tcf1 protein downregulation occurred with similar kinetics (Figure S2A), in agreement with (Lin et al., 2016; Gulliksrud et al., 2017). The d8 *Tcf7*^{GFPhi} cells highly expressed Tcf1 protein, while cells with intermediate *Tcf7*^{GFP} expression showed reduced amounts of Tcf1, and most *Tcf7*$^{GFP-}$ cells lacked Tcf1 protein (Figure 1B). Despite the decreasing frequency, the abundance of *Tcf7*^{GFPhi} cells increased 1,000-fold from d0 to d8 but changed minimally following pathogen clearance (∼2-fold decrease) from d8 to d50 p.i. (Figure 1C). In comparison, P14 cells with a KLRG1− CD127+ memory precursor (MP) phenotype contracted 13-fold (Figure 1D). Although 73% of d8 *Tcf7*^{GFPhi} cells had an MP phenotype (Figure S2B), only around 10% of MP cells were *Tcf7*^{GFPhi} (Figure 1E). This showed that MP cells were heterogeneous and suggested that only the *Tcf7*^{GFPhi} MP subset efficiently formed memory. Indeed, d8 *Tcf7*^{GFPhi} cells showed efficient survival *in vitro* and limited cycling *ex vivo* (Figures S2C and S2D). On d6 p.i., only half of *Tcf7*^{GFPhi} cells had an MP phenotype, and most *Tcf7*^{GFPhi} cells were KLRG1− CD127− on d4 p.i. (Figure S2B). Thus, *Tcf7*^{GFPhi} and *Tcf7*$^{GFP-}$ cells diverged prior to and independent from the emergence of an MP phenotype.

D8 *Tcf7*^{GFPhi} cells overexpressed certain markers of human stem-cell-like memory cells (Tscm), such as Sca-1 or CXCR3 (Figure S2E) (Gattinoni et al., 2011), and expressed the central memory markers *Ccr7* (Figure S2F) and CD62L (Figure 1F), whereby a discrete CD62L+ subset was detected throughout the early response (Figure S2G). Furthermore, d8 *Tcf7*^{GFPhi} cells produced >4-fold more IL-2 than did *Tcf7*$^{GFP-}$ cells, while IFN-γ and TNF-α production was equivalent (Figure 1G). Increased IL-2 production by *Tcf7*^{GFPhi} cells was already evident on d4 p.i. (Figure S2H). Polyclonal d8 *Tcf7*^{GFPhi} CD8+ T cells specific for two distinct LCMV epitopes displayed corresponding phenotypic and functional characteristics (Figures S3A–S3E).

(B) Tcf1 protein expression by sorted *Tcf7*^{GFP}-defined P14 cells at day 8 (d8) p.i. compared to *Tcf7*$^{−/−}$ (KO) P14 cells (gray fill).
(C) Abundance of *Tcf7*^{GFPhi} (green) and *Tcf7*$^{GFP-}$ P14 cells (blue) and of (D) KLRG1− CD127+ memory precursor (MP) (gray) or KLRG1+ CD127− terminal effector (TE) (purple) P14 cells. Numbers indicate the fold difference between d8 and d50. (E) *Tcf7*^{GFP} expression by gated TE or MP cells at d8 p.i.
(F–J) Analysis of d8 *Tcf7*^{GFPhi} and *Tcf7*$^{GFP-}$ P14 cells for (F) CD127 and CD62L, (G) cytokine production, (H) lytic activity against gp33-peptide pulsed tumor cells, (I) LAMP-1 (CD107a) release, and (J) GzmA and GzmB protein expression.
(K–O) Spleen cross sections at d8 p.i. were stained for (K and L) CD45.2 (P14 cells) (blue), GFP (*Tcf7*^{GFP}) (green), CD4 (red), and DAPI (gray). Scale bar, 500 μm. (M) Higher magnification of the indicated region (scale bar, 100 μm), (N) with further magnification of the original immunofluorescence staining (top) and the digital image (bottom) to identify *Tcf7*$^{GFP+}$ and *Tcf7*$^{GFP-}$ P14 cells among nucleated cells (DAPI+). Scale bar, 50 μm. (O) Abundance of d8 *Tcf7*$^{GFP+}$ or *Tcf7*$^{GFP-}$ P14 cells in the B cell zone (blue), the T cell zone (pink), and the red pulp (gray) based on image analysis.
Data are compiled from 2 experiments with 6–9 mice per time point (A), representative of 3 experiments (B), of 2 experiments with 3–5 mice per group (C, D, G, H, and J), of 5 experiments with 4 mice per group (E and F), or from one experiment with 5 mice (I). Data in (K–O) are representative of 4 cross-sections from 4 different mice. Mean ± SD are shown. Statistics: non-paired two-tailed Student's test (F, G, I, J, and O) or two-way ANOVA with Sidak's test (H) with ***p < 0.001; ****p < 0.0001, and (ns) p > 0.05. See also Figures S1–S4.
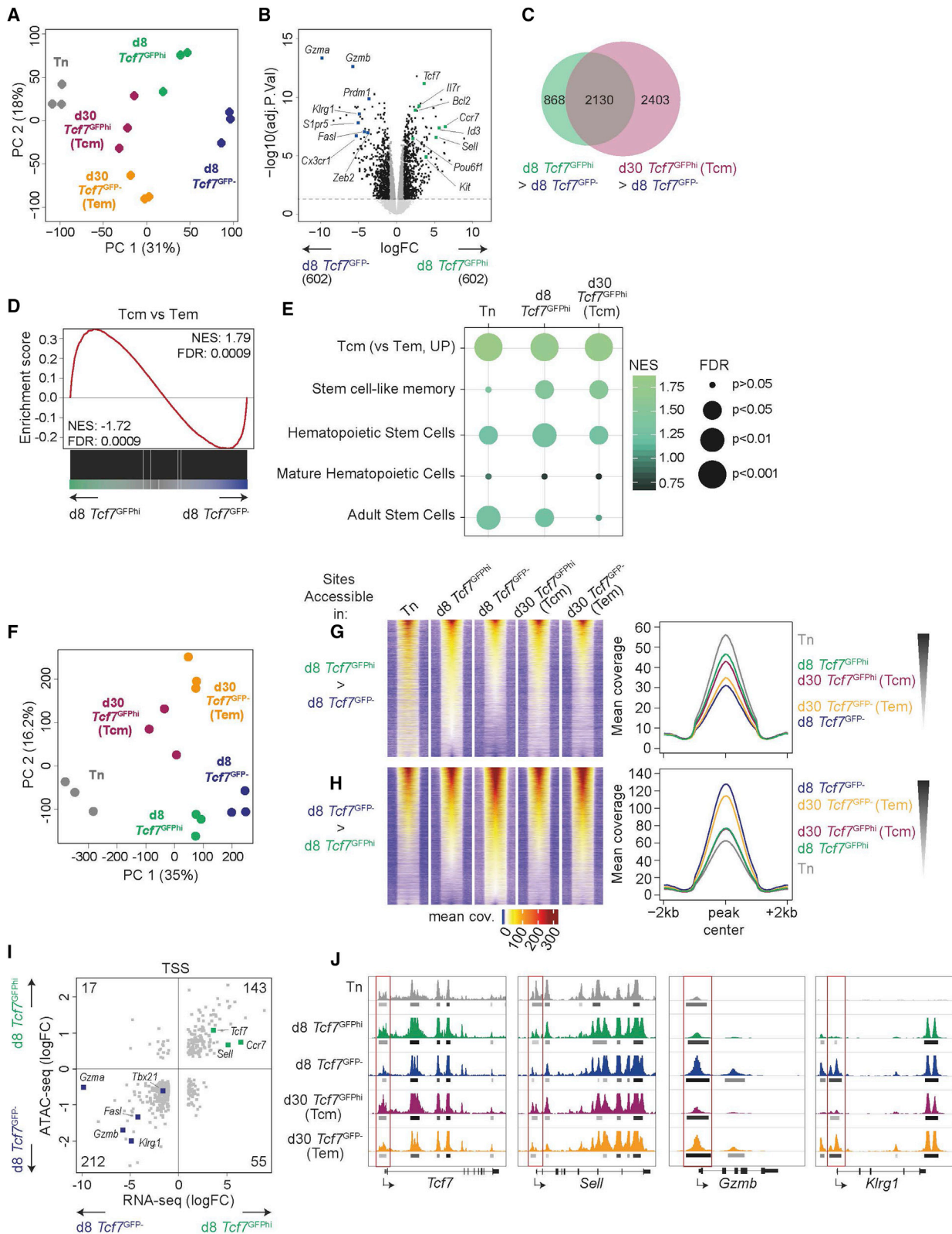
Figure 2. Gene Expression and Chromatin Accessibility Analysis of d8 *Tcf7*^GFPhi Cells

Sorted Tn, d8, and d30 *Tcf7*^GFPhi and *Tcf7*^GFP- P14 cells were subjected to (A–E) RNA-seq or (F–J) ATAC-seq analysis.

(A) Principal component analysis (PCA) of gene expression counts from the indicated populations of cells. Each dot represents a biological replicate.

(legend continued on next page)

While d8 *Tcf7*^GFP- cells were highly cytolytic, *Tcf7*^GFPhi cells essentially failed to kill target cells (Figure 1H). This contrasts with MP cells, which efficiently kill target cells (Joshi et al., 2007). Deficient killing was not due to reduced T cell receptor (TCR) signaling or impaired exocytosis of granules, since d8 *Tcf7*^GFPhi cells efficiently produced IFN-γ and TNF-α (Figure 1G) and mobilized LAMP-1 (CD107a) (Figure 1I). Rather, d8 *Tcf7*^GFPhi cells expressed very little *Gzma*, *Gzmb*, Perforin (*Prf1*), and Fas ligand (*Fasl*) mRNA (Figure S3F), and few cells expressed GzmA and GzmB protein (Figure 1J). Although subsets of *Tcf7*^GFPhi cells transiently expressed GzmB between d2 and d4 p.i., most *Tcf7*^GFPhi cells lacked GzmB, and GzmA was never expressed (Figure S3G). Thus, *Tcf7* expression demarcated rare effector-phase CD8+ T cells that resembled Tcm cells, lacked cytolytic activity, and did not contract following pathogen clearance.

Effector-Stage *Tcf7*^GFP+ and Tcm Cells Exhibit Comparable Distribution in the Spleen

We further determined the presence of *Tcf7*^GFPhi cells in various tissues. D8 *Tcf7*^GFPhi cells were detected in hematopoietic tissues (spleen, lymph node [LN], bone marrow [BM]), in the circulation (peripheral blood) and in the parenchyma of non-hematopoietic tissues (lung, intra epithelial lymphocytes [IEL]) (Figure S4A). We used multicolor immunofluorescence staining combined with digital image analysis to determine the anatomical location of *Tcf7*^GFP+ cells in the spleen at d8 p.i. (Figures 1K–1O). The abundance of *Tcf7*^GFP+ P14 cells detected *in situ* corresponded to that obtained after tissue homogenization and flow cytometric analysis (Figure S4B). The vast majority of d8 *Tcf7*^GFP- P14 cells localized to the splenic red pulp (~90%) with fewer cells located in the T cell zone (10%). In contrast, 40% of d8 *Tcf7*^GFP+ P14 cells localized to the T cell zone, 3% to the B cell zone, and 57% to the red pulp (Figure 1O). A similar distribution was observed for d30 *Tcf7*^GFP+ (Tcm) P14 cells, while naive *Tcf7*^GFP+ (Tn) P14 cells preferentially localized to the T cell zone (Figure S4C). Splenic d8 *Tcf7*^GFP+ and d30 *Tcf7*^GFP+ (Tcm) cells thus showed a comparable localization.

Effector-Stage *Tcf7*^GFPhi and Tcm Cells Show Comparable Expression and Accessibility of Lineage-Specific Loci

We further addressed the relatedness of d8 *Tcf7*^GFPhi and d30 *Tcf7*^GFPhi (Tcm) cells using gene expression and chromatin accessibility analyses. Principal component analysis (PCA) of RNA-seq data showed that d8 *Tcf7*^GFPhi cells clustered closer to d30 *Tcf7*^GFPhi (Tcm) than to d8 *Tcf7*^GFP- or d30 *Tcf7*^GFP- (Tem) cells (Figure 2A). Indeed, d8 *Tcf7*^GFPhi cells overexpressed

multiple Tcm-associated genes (*Tcf7, Ccr7, Sell, Il7r, Id3*), whereas *Tcf7*^GFP- cells were enriched in effector-gene expression (*Gzma, Gzmb, Fasl, Klrg1, Prdm1*) (Figures 2B and S4D) (Table S1).

D8 *Tcf7*^GFPhi and d30 *Tcf7*^GFPhi (Tcm) cells shared a substantial number of differentially expressed genes (40%) (Figure 2C), and their similarity was confirmed using gene set enrichment analysis (GSEA) (Figure S4E) and corroborated using an independent Tcm signature (Mackay et al., 2016) (Figures 2D and 2E). Furthermore, the transcriptome of d8 *Tcf7*^GFPhi cells overlapped with a stem-cell-like memory signature (Pace et al., 2018), an adult stem-cell signature (Wong et al., 2008), and a hematopoietic stem and progenitor cell signature, but not with a mature hematopoietic cell signature (Ivanova et al., 2002) (Figures 2E and S4F). Most of the enrichments were also observed with d30 *Tcf7*^GFPhi (Tcm) and Tn cells (Figure 2E). Thus, effector-stage *Tcf7*^hi CD8+ T cells were transcriptomically similar to Tcm and Tn, but different from *Tcf7*⁻ Teff or Tem cells.

We further compared the epigenetic landscape of CD8+ T cell subpopulations using ATAC-seq. PCA of differentially accessible chromatin regions showed that d8 *Tcf7*^GFPhi and d30 *Tcf7*^GFPhi (Tcm) cells clustered closer to Tn than d8 *Tcf7*^GFP- and d30 *Tcf7*^GFP- (Tem) cells (Figure 2F). Between d8 *Tcf7*^GFPhi and *Tcf7*^GFP- cells, a total of 17,676 chromatin regions were differentially accessible (FDR [false discovery rate] p < 0.05). Regions more accessible in d8 *Tcf7*^GFPhi cells were also more accessible in d30 *Tcf7*^GFPhi (Tcm) and Tn cells but were less accessible in d30 *Tcf7*^GFP- (Tem) cells (Figure 2G). Conversely, regions more accessible in d8 *Tcf7*^GFP- cells were more accessible in d30 *Tcf7*^GFP- (Tem) cells but less accessible in d30 *Tcf7*^GFPhi (Tcm) and Tn cells (Figure 2H). Thus, the chromatin accessibility of d8 *Tcf7*^GFPhi cells was globally similar to that of Tcm and Tn cells but different from d8 *Tcf7*^GFP- and Tem cells, similar to the gene expression analysis.

To identify functionally relevant accessibility changes, we integrated our RNA-seq and ATAC-seq datasets. Focusing on the transcriptional start site (TSS) identified 4,049 genes with differential TSS accessibility in d8 *Tcf7*^GFPhi compared to *Tcf7*^GFP- cells (FDR p < 0.05) (Table S2). The TSS was significantly more accessible in 143 of the 602 genes (23.8%) that were overexpressed in d8 *Tcf7*^GFPhi cells (Figure 2I) (Table S3). These genes included central memory genes such as *Tcf7, Sell*, or *Ccr7* (Figures 2I and 2J) (Table S3). More than half of this class of genes was also more accessible in d30 *Tcf7*^GFPhi (Tcm) cells (74 of 143) (Figure S4G), as illustrated in (Figure 2J). This suggested that accessibility of the TSS contributed to the increased expression of central memory genes in d8 *Tcf7*^GFPhi cells and that their downregulation in *Tcf7*^GFP- cells was due to reduced TSS accessibility.

(B) Differentially expressed genes (DEGs) between d8 *Tcf7*^GFPhi and *Tcf7*^GFP- cells (log$_2$ FC > 1 and adj. p < 0.05).
(C) DEG between d8 *Tcf7*^GFPhi and d30 *Tcf7*^GFPhi cells, relative to d8 *Tcf7*^GFP- cells.
(D and E) Gene set enrichment analysis (GSEA) of (D) d8 *Tcf7*^GFPhi versus d8 *Tcf7*^GFP- cells against a Tcm versus Tem cell signature. (E) GSEA results of Tn, d8 *Tcf7*^GFPhi and d30 *Tcf7*^GFPhi cells (each versus d8 *Tcf7*^GFP- cells) testing enrichment in the indicated gene signatures. Dot sizes and color scales are proportional to the false discovery rate (FDR) and the normalized enrichment score (NES), respectively.
(F–J) ATAC-seq analysis. (F) PCA of accessible regions in the indicated populations of cells. Each dot represents a biological replicate. (G and H) Peak centered heatmaps of ATAC-seq read coverage. The coverage of regions more accessible in d8 *Tcf7*^GFPhi cells (G) or in d8 *Tcf7*^GFP- cells (H) are shown for Tn, d30 *Tcf7*^GFPhi (Tcm), and d30 *Tcf7*^GFP- (Tem) cells and are sorted according to their extent of coverage in d8 *Tcf7*^GFPhi and *Tcf7*^GFP- cells. Line graphs show the corresponding mean intensity of the read coverage. (I) Differentially accessible transcription start sites (TSSs) in d8 *Tcf7*^GFPhi versus d8 *Tcf7*^GFP- cells (FDR p < 0.05) were correlated with gene expression data (log$_2$FC > 1 and adj. p < 0.05). (J) Read coverage track for the indicated memory and effector genes. The region surrounding the TSS is highlighted using a red outline. Horizontal lines depict accessible regions based on peak calling. See also Figure S4.
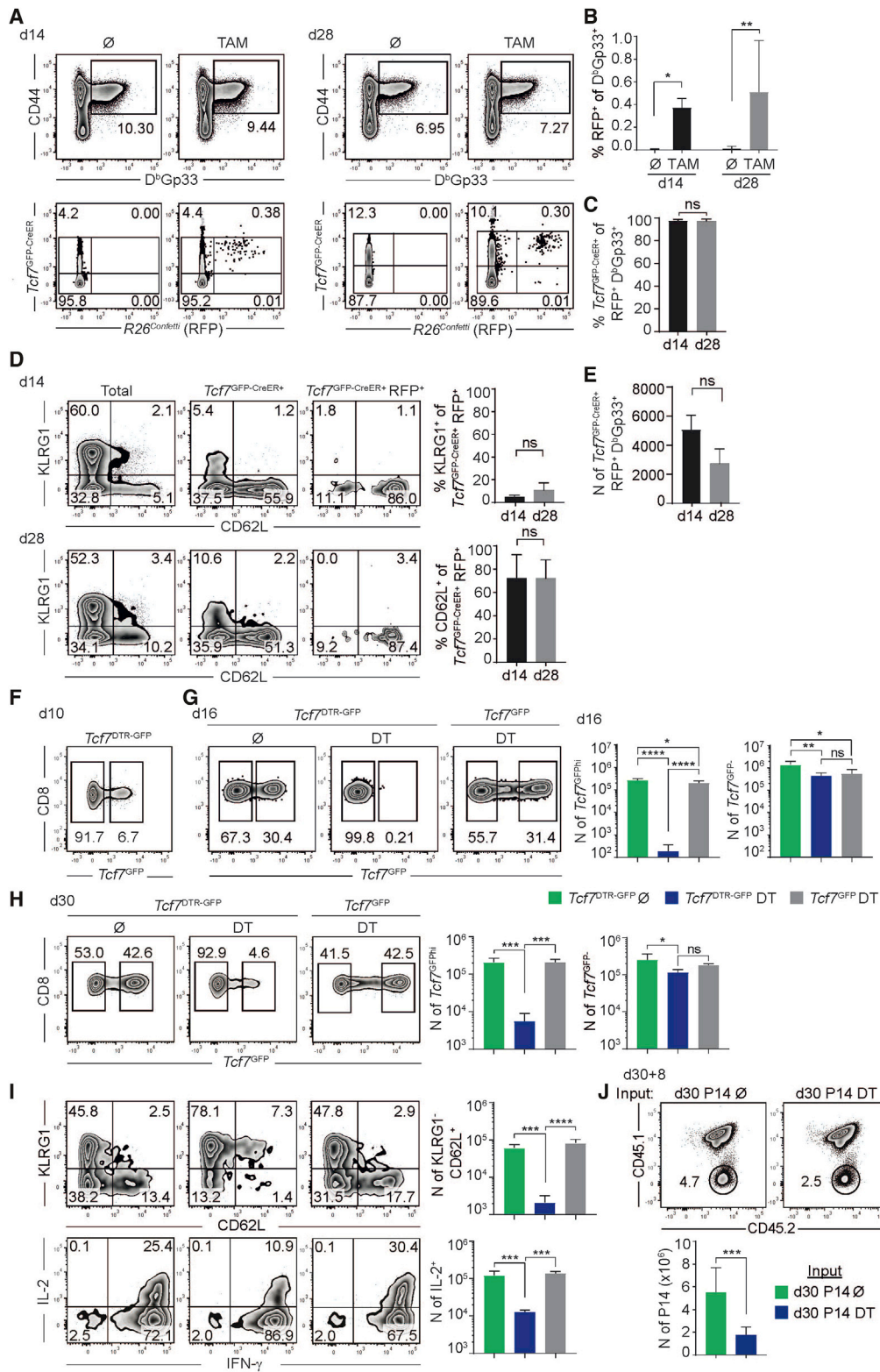
Figure 3. Fate Mapping and Ablation of *Tcf7*^GFPhi Cells to Determine the Origin of Tcm Cells

(A–E) *Tcf7*^GFP-CreER *R26*^Confetti mice were infected with LCMV WE and left untreated (Ø) or were injected with Tamoxifen (TAM) starting on d8 p.i. (A) *Tcf7*^GFP-CreER (intermediated amounts of GFP, see STAR Methods for further explanation) and *R26*^Confetti (RFP) expression by D^bGp33 tetramer^+ CD44^+ CD8^+ T cells on d14 (left) or d28 p.i. (right). (B) Fraction of RFP^+ cells among D^bGp33^+ cells and (C) of *Tcf7*^GFP-CreER+ RFP^+ cells among RFP^+ cells. (D) Expression of KLRG1 and CD62L

(legend continued on next page)

Conversely, the TSS was more accessible in 212 of the 602 (35.2%) genes that were overexpressed in d8 $Tcf7^{GFP-}$ cells (Table S3). The d8 $Tcf7^{GFP-}$ program included effector genes such as *Gzmb, Klrg1, Fasl, Cx3cr1, Tbx21* (T-bet), *and Runx1* (Table S3) (Figures 2I and 2J). The acquisition of this program was therefore explained in part by increased TSS accessibility, while low expression of this class of genes in d8 $Tcf7^{GFPhi}$ cells was explained by reduced TSS accessibility. As one example, the *Gzmb* locus was accessible in d8 $Tcf7^{GFP-}$ and Tem cells but essentially inaccessible in d8 $Tcf7^{GFPhi}$ and Tcm cells (Figure 2J). Of note, prior work suggested that effector loci, including *Gzmb,* are accessible in MP and memory cells (Jadhav et al., 2019; Scott-Browne et al., 2016; Wang et al., 2018). However, these studies did not distinguish Tcm and Tem cells, and we found that MP cells are heterogenous. When the respective compartments were separated into $Tcf7^{hi}$ and $Tcf7^-$ cells, effector loci were poorly accessible in $Tcf7^{hi}$ cells (Figure 2J), suggesting that these cells had not passed through a cytolytic differentiation state, in agreement with our flow cytometric analysis (Figure S3G). Overall, the expression and accessibility of lineage-specific loci were similar in d8 $Tcf7^{GFPhi}$, d30 $Tcf7^{GFPhi}$ (Tcm) and Tn cells and different from d8 $Tcf7^{GFP-}$ and d30 $Tcf7^{GFP-}$ (Tem) cells.

Tcm Cells Quantitatively Derive from Effector-Stage $Tcf7^{GFPhi}$ CD8+ T Cells

To determine the fate of effector-stage $Tcf7^+$ CD8+ T cells, we generated a $Tcf7^{GFP-CreER}$ mouse strain (Figure S5A) that we crossed to $Rosa26^{lox\ stop\ lox\ Confetti}$ ($R26^{Confetti}$) reporter mice. Tamoxifen (TAM)-mediated induction of Cre recombinase activity in $Tcf7^+$ cells resulted in the stochastic and mutually exclusive expression of one of four fluorescent proteins (RFP, CFP, YFP, or GFP), whereby only RFP expression is shown. GFPhi cells, which appeared following TAM injection and which could be discriminated from the $Tcf7^{GFP-CreER+}$ cells (see STAR Methods for further explanation), were removed from the analysis. The $Tcf7^{GFP-CreER}$ construct was expressed by virtually all CD8+ T cells from naive mice, downregulated in most CD8+ T cells responding to LCMV infection (Figures S5B and S5C), whereby residual d8 $Tcf7^{GFP-CreER+}$ cells identified Tcf1 protein-expressing cells (Figure S5D).

LCMV-infected $Tcf7^{GFP-CreER}$ $R26^{Confetti}$ mice were injected with TAM starting at d8 p.i. Two days after the last injection (d14), H-2D^b Gp33 tetramer$^+$ (D^{b}Gp33$^+$) CD8$^+$ T cells contained a small population of RFP$^+$ cells (0.38% of CD8), while RFP$^+$ cells were not detected in the absence of TAM (Figures 3A and 3B) or in TAM-treated mice that harbored only the $R26^{Confetti}$ allele (Figure S5E). The vast majority of d14 RFP$^+$ cells were $Tcf7^{GFP-CreER+}$, which expressed intermediated amounts of GFP (see STAR Methods for further explanation) (Figures 3A and 3C). This demonstrated the selective labeling of

$Tcf7^{GFP-CreER+}$ cells and the absence of their differentiation into $Tcf7^{GFP-CreER-}$ cells between d8 and d14 p.i. Furthermore, most of the d14 RFP$^+$ $Tcf7^{GFP-CreER+}$ cells were KLRG1$^-$ CD62L$^+$ (Figure 3D). At d28 p.i., D^{b}Gp33$^+$ RFP$^+$ cells were still uniformly $Tcf7^{GFP-CreER+}$, and most cells had a KLRG1$^-$ CD62L$^+$ Tcm phenotype (Figures 3A–3D). Importantly, the abundance of D^{b}Gp33$^+$ RFP$^+$ $Tcf7^{GFP-CreER+}$ cells at d14 and d28 p.i. was not different (Figure 3E). Corresponding data were obtained for polyclonal D^{b}Np396$^+$ CD8$^+$ T cells (Figure S5F) and for monoclonal P14 $Tcf7^{GFP-CreER}$ $R26^{Confetti}$ cells (Figures S5G–S5I). Thus, d8 $Tcf7^+$ cells maintained $Tcf7$ expression and quantitatively yielded Tcm cells, indicating that effector-stage $Tcf7^+$ cells represent central memory precursors.

We further determined whether $Tcf7$-negative cells contributed to the central memory compartment. To this end, we ablated $Tcf7^{DTR-GFP+}$ cells *in vivo* using diphtheria toxin (DT) administration (Siddiqui et al., 2019). Naive $Tcf7^{DTR-GFP}$ P14 cells were transferred into B6 recipients, which were infected with LCMV. DT treatment was started at d10, when 6.7% of P14 cells were $Tcf7^{DTR-GFP+}$ (Figure 3F), and mice were analyzed one day after the last injection (d16). DT treatment profoundly depleted $Tcf7^{DTR-GFP+}$ but not $Tcf7^{DTR-GFP-}$ cells, compared to DT treated mice harboring control $Tcf7^{GFP}$ cells (Figure 3G). The spleen of treated mice contained very few $Tcf7^{DTR-GFP+}$ P14 cells (190 ± 167) at d16 but contained significantly more $Tcf7^{DTR-GFP+}$ cells (5,542 ± 3,416) (p < 0.01) at d30 p.i. (Figure 3H). It was thus possible that $Tcf7$ was re-expressed by previously $Tcf7$-negative cells. However, even if that was the case, the contribution of such cells to the normal $Tcf7^+$ memory compartment (2.1 ± 0.4 × 10^5 cells) was minor (2.7%). On the other hand, DT-treated mice harbored comparable numbers of $Tcf7^{DTR-GFP-}$ and control $Tcf7^{GFP-}$ memory cells at d30 p.i. (Figure 3H), suggesting that $Tcf7^+$ cells did not contribute to the $Tcf7^-$ memory pool after d16 p.i.

The analysis of the memory compartment showed that DT treatment strongly reduced the abundance of CD62L$^+$ KLRG1$^-$ memory cells (39-fold) (Figure 3I) or of IL-2$^+$ cells (10-fold) (Figure 3I) and the recall expansion capacity (3-fold) (Figure 3J). Thus, ablation of d10–15 $Tcf7^+$ cells blunted central memory functions. Earlier ablation of $Tcf7^+$ cells (from d6 to d9 p.i.) yielded overall similar results (Figures S5J–S5L), even though these DT-treated mice became sick (independent of the depletion of $Tcf7^{DTR-GFP}$ cells) and had to be analyzed by d16 p.i. We concluded that central memory derived almost exclusively from effector-stage $Tcf7^+$ cells.

Effector-Stage $Tcf7^{GFPhi}$ CD8+ T Cells Have Central Memory Function

Memory-biased effector-phase CD8+ T cells are thought to acquire central memory functions following antigen clearance, i.e., late during the contraction phase (Kaech et al., 2002). We

by D^{b}Gp33$^+$ (left), D^{b}Gp33$^+$ $Tcf7^{GFP-CreER+}$ (center) and D^{b}Gp33$^+$ $Tcf7^{GFP-CreER+}$ RFP$^+$ cells (right) on d14 (top) and d28 p.i. (bottom). (E) Abundance of D^{b}Gp33$^+$ $Tcf7^{GFP-CreER+}$ RFP$^+$ cells at d14 and d28 p.i.

(F–J) $Tcf7^{DTR-GFP}$ or control $Tcf7^{GFP}$ P14 cells (CD45.2) were transferred into B6 mice (CD45.1/.2) that were infected with LCMV Arm and injected with PBS (Ø) or diphtheria toxin (DT) starting on d10 p.i. (F). Abundance of $Tcf7^{DTR-GFP}$ (or control $Tcf7^{GFP}$) P14 cells in the spleen on d16 (G) and d30 p.i. (H). (I) KLRG1 versus CD62L (top) and IL-2 versus IFN-γ expression (bottom) on d30 p.i. (J) Recall response on d8 post-challenge of d30 P14 cells sorted from untreated (Ø) and DT treated mice (DT) (d30+8).

Data are pooled from 3 experiments with 5–6 mice per group (A–E), compiled from 2 experiments with 5 mice per group (G), or representative of 2 experiments with 4–5 mice per group (H–J). Mean ± SD are shown. Statistics: non-paired two-tailed Student's test (A–E and J) or on one-way ANOVA with Tukey's test (G–I) with *p < 0.05; **p < 0.01; ***p < 0.001; and (ns) p > 0.05. See also Figure S5.
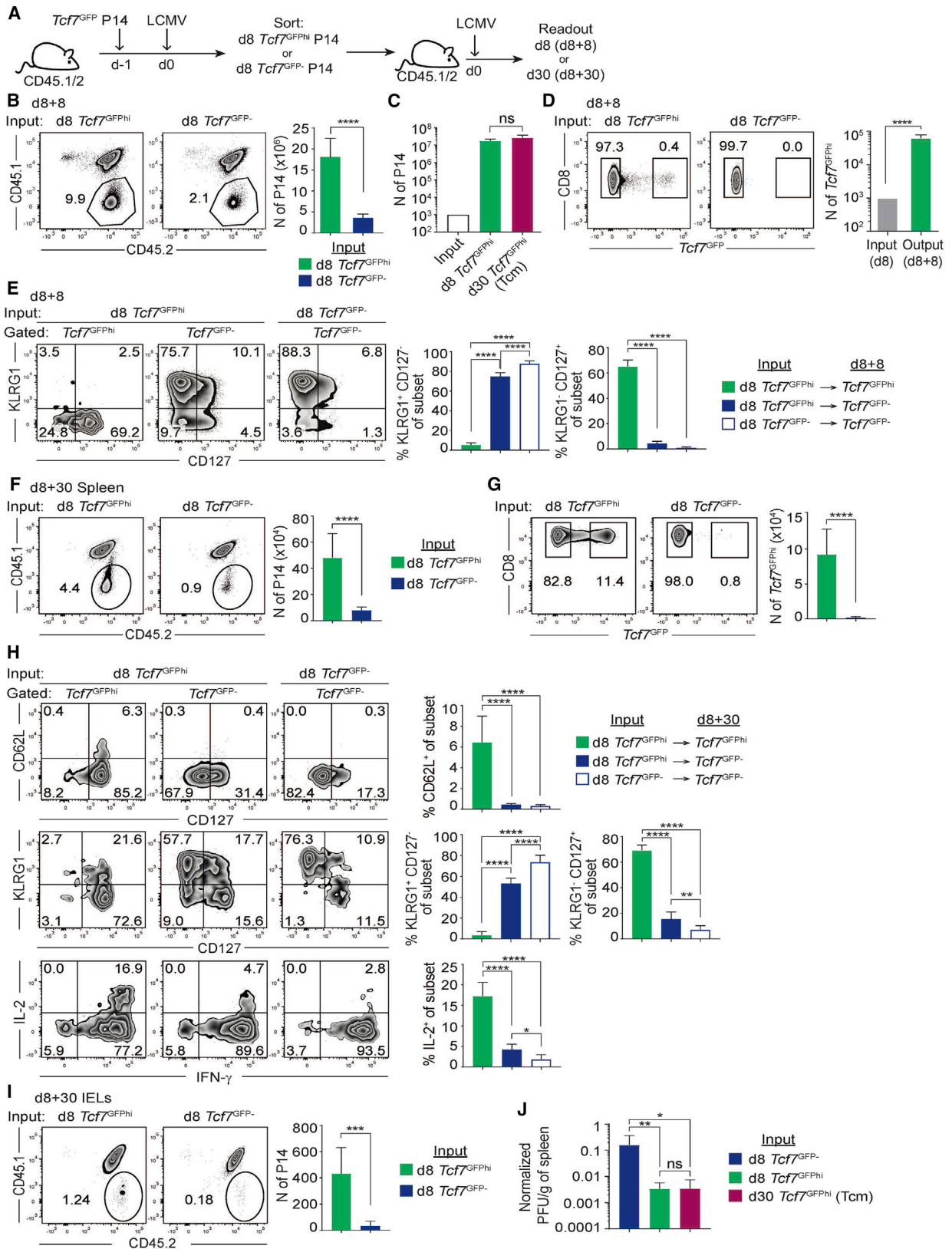
(legend on next page)

thus tested whether d8 *Tcf7*^{GFPhi} CD8⁺ T cells indeed lacked Tcm function (as schematically shown in Figure 4A). Compared to *Tcf7*^{GFP-} cells, flow-sorted d8 *Tcf7*^{GFPhi} cells mediated an efficient recall response (Figure 4B), which was virtually identical to that of d30 *Tcf7*^{GFPhi} (Tcm) cells (Figure 4C). Progeny of d8 *Tcf7*^{GFPhi} cells were mostly *Tcf7*^{GFP-} terminal effector (TE) cells, but secondary *Tcf7*^{GFPhi} cells with a predominant MP phenotype were also detected (Figures 4D and 4E). The abundance of secondary *Tcf7*^{GFPhi} cells was significantly increased compared to input (Figure 4D), indicating that *Tcf7*^{GFPhi} cells reproduced. Conversely, descendants of d8 *Tcf7*^{GFP-} cells remained *Tcf7*^{GFP-} and displayed a TE phenotype (Figures 4D and 4E), indicating that *Tcf7* expression was stably extinguished. Corresponding results were obtained for polyclonal d8 *Tcf7*^{GFPhi} CD8⁺ T cells specific for two distinct LCMV epitopes (Figures S6A–S6E).

To formally address whether d8 *Tcf7*^{GFPhi} cells self-renewed, we performed tertiary transfers (Figures S6F–S6H). Secondary *Tcf7*^{GFPhi} P14 cells (d8+8) retained recall expansion capacity (Figure S6F) and produced both *Tcf7*^{GFP-} as well as tertiary *Tcf7*^{GFPhi} cells that displayed a predominant MP phenotype and that had expanded compared to input (Figures S6G and S6H). Thus, serial transfers showed that effector-stage *Tcf7*^{GFPhi} cells had expansion, self-renewal, and differentiation capacity.

To address multi-potency, the response of d8 *Tcf7*^{GFPhi} cells was analyzed 30 days after recall stimulation (d8+30). Compared to d8 *Tcf7*^{GFP-} cells, d8 *Tcf7*^{GFPhi} cells yielded significantly larger memory compartments in both hematopoietic and non-hematopoietic tissues (Figure 4F, 4I, S6I, and S6K). D8 *Tcf7*^{GFPhi} cells yielded Tcm (CD127⁺ CD62L⁺, IL-2⁺, *Tcf7*^{GFPhi}) and Tem cells (CD127 [±] CD62L⁻, *Tcf7*^{GFP-}) in spleen and LN (Figure 4G, 4H, and S6J) as well as tissue-resident memory cells (Trm) among intraepithelial lymphocytes (IELs) in the small intestine and in the lung (Figures 4I and S6K). In comparison, d8 *Tcf7*^{GFP-} cells yielded considerably fewer Trm and Tem cells and essentially failed to yield Tcm cells (Figures 4F–4I and S6I–S6K). Thus, d8 *Tcf7*^{GFPhi} cells yielded all memory populations as well as Teff cells, indicative of multi-lineage differentiation potential. Finally, we tested the capacity of d8 *Tcf7*^{GFPhi} cells to protect from viral infection. Adoptive transfer of d8 *Tcf7*^{GFPhi} P14 cells into Vβ5 TCR transgenic mice, which cannot control viral infection, reduced splenic virus titers to the same extent as did d30 *Tcf7*^{GFPhi} (Tcm) cells and more efficiently than did d8 *Tcf7*^{GFP-} cells (Figure 4J). Together, these data show that effector-stage *Tcf7*^{GFPhi} cells have key hallmarks associated with central memory cells.

Tcf1^{hi} CD8⁺ T Cells Are Present during the Acute Response to Vaccination in Mice and Humans

We next addressed whether *Tcf7*^{GFPhi} CD8⁺ T cells could be generated by vaccination. To this end, we primed (d0) and boosted (d14) *Tcf7*^{GFP} mice using a modified Ovalbumin (Ova) peptide mixed with Pam3CSK4 (TLR1 and 2 agonist) and emulsified in Montanide (Figure 5A). We detected H-2K^b Ovalbumin tetramer⁺ (K^bOva⁺) *Tcf7*^{GFPhi} CD62L⁺ CD8⁺ T cells in the peripheral blood of vaccinated mice one week after the boost (d21) (Figures 5B–5D). Such cells were equally abundant 3 weeks after the boost in blood (d35) (Figures 5C and 5D), were also detected in the spleen (Figures 5E–5G), and were further shown to produce IL-2 (Figure 5H). Thus, endogenous antigen-specific *Tcf7*^{hi} CD8⁺ T cells were detectable shortly after vaccination, and such cells persisted, although they were rare compared to natural infection.

We also addressed whether TCF1^{hi} CD8⁺ T cells were detectable during an acute response in human volunteers exposed to the live-attenuated yellow fever virus vaccine YF-17D. Peripheral blood of human vaccinees (n = 6) was analyzed for the presence of HLA-A*02-restricted CD8⁺ T cells specific for the viral LLWNGPMAV peptide (LLW). At d14 post-vaccination, i.e., the peak of the response, most A2/LLW tetramer⁺ CD8⁺ T cells were TCF1^{lo} compared to naive CD8⁺ T cells (Figures 5I and 5J), and these TCF1^{lo} cells had a predominant Tem (CCR7⁻ CD45RA⁻) phenotype (Figures 5I and 5K). However, we also detected TCF1^{hi} A2/LLW⁺ CD8⁺ T cells in all donors, and these had a predominant Tcm (CCR7⁺ CD45RA⁻) and, to a lesser extent, a Tscm (CCR7⁺ CD45RA⁺ CD95⁺) phenotype (Figures 5I–5K). Thus, TCF1^{hi} CD8⁺ T cells with a central memory phenotype existed at the peak of the acute response to vaccination in humans.

Tcf1 Ensures Stemness of Effector-Stage *Tcf7*^{GFPhi} CD8⁺ T Cells

To address the importance of Tcf1 in the generation and/or the function of d8 *Tcf7*^{GFPhi} cells, we generated *Tcf7*^{−/−} *Tcf7*^{GFP} reporter mice. *Tcf7*^{−/−} reporter P14 cells highly expressed *Tcf7*^{GFP} (Figure S7A), indicating that reporter activity did not depend on Tcf1 protein.

Naive wild-type (WT) and *Tcf7*^{−/−} reporter P14 cells gave rise to equivalent or modestly reduced populations of total P14 and of *Tcf7*^{GFPhi} P14 cells at d8 p.i. (Figures 6A and 6B). While there were no evident differences between WT and *Tcf7*^{−/−} *Tcf7*^{GFP-} cells (Figure S7B), *Tcf7*^{−/−} *Tcf7*^{GFPhi} cells expressed significantly more KLRG1 but less CD62L (Figure 6C) and less IL-2 compared to WT (Figure 6D), whereas IFN-γ and TNF-α expression was

---

Figure 4. Effector-Stage *Tcf7*^{GFPhi} Cells Have Central Memory Function

(A) Recall response and memory formation by sorted d8 *Tcf7*^{GFPhi} or *Tcf7*^{GFP-} P14 cells.

(B and C) Abundance on d8 post-challenge of d8 *Tcf7*^{GFPhi} P14 cells (B) compared to that of d30 *Tcf7*^{GFPhi} (Tcm) cells (C).

(D and E) Abundance of secondary *Tcf7*^{GFPhi} P14 cells compared to input (D) and KLRG1 versus CD127 expression (E).

(F and G) Abundance of P14 cells (F) and of *Tcf7*^{GFPhi} P14 cells (G) on d30 post-challenge of d8 *Tcf7*^{GFPhi} or *Tcf7*^{GFP-} cells (d8+30).

(H) Phenotype (top & middle) and IL-2 and IFN-γ production (bottom) by d8+30 *Tcf7*^{GFPhi} and *Tcf7*^{GFP-} memory cells.

(I) Abundance of memory cells derived from d8 *Tcf7*^{GFPhi} cells (d8+30) among intraepithelial lymphocytes of the small intestine.

(J) The indicated population of cells were transferred into Vβ5 TCR transgenic mice that were then infected with LCMV Arm. Plaque-forming units (PFUs) per gram of spleen were determined on d8 p.i. and normalized to no cell transfers.

Data in (B, C, D, and E) are representative of 2 experiments with 5–7 mice per group, compiled from 3 experiments with 11–12 mice per group (F, G, and H), compiled from 2 experiments with 6 mice per group (I), or compiled from 2 experiments with 10–11 mice per group (J). Mean ± SD are shown. Statistics: non-paired t test (B, D, F, G, and I) or one-way ANOVA with Tukey's test (C, E, H, and J) with ***p < 0.001; ****p < 0.0001; and (ns) p > 0.05. See also Figure S6.
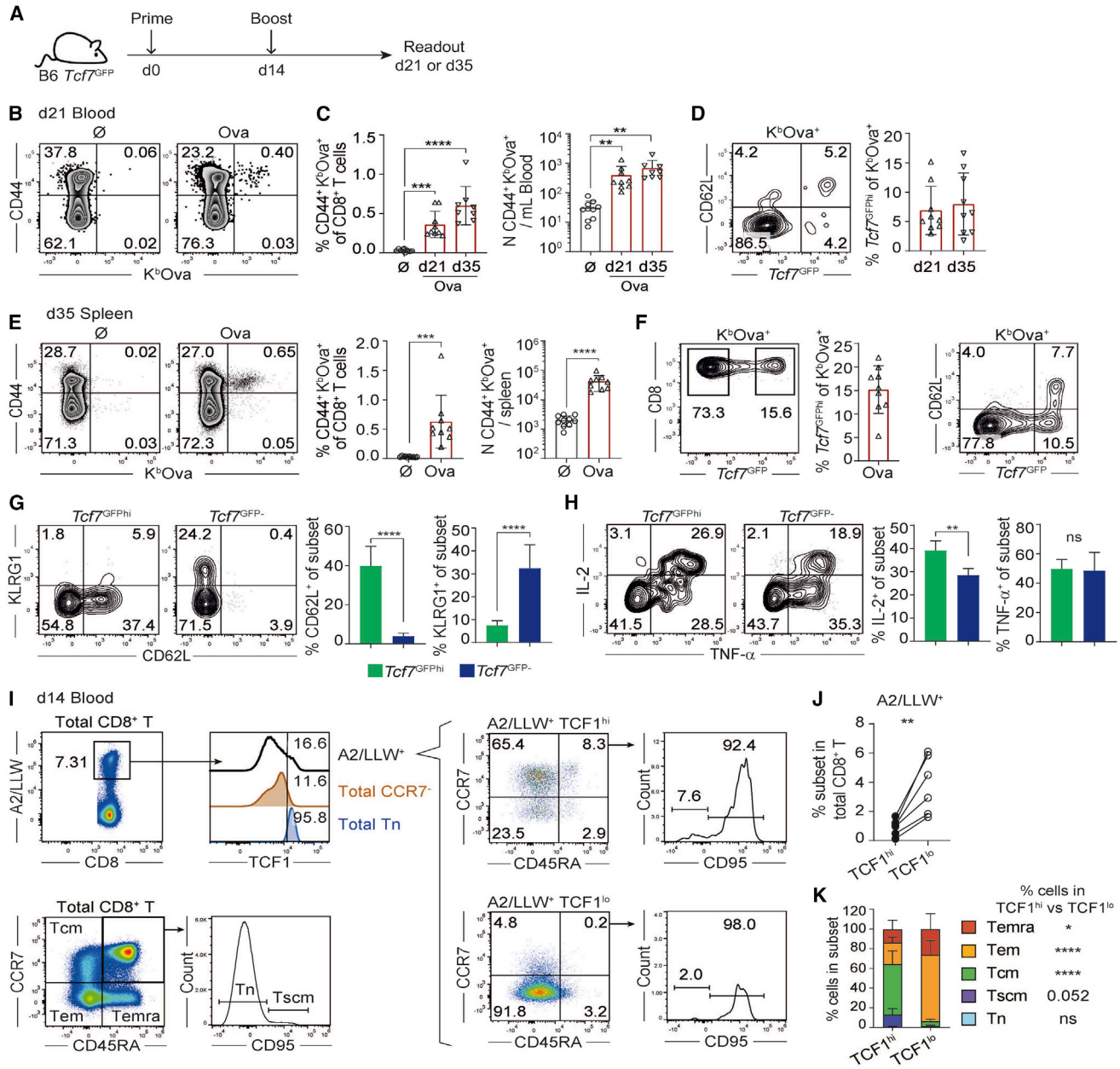
Figure 5. Vaccination of Mice and Humans Generates Effector-Phase Tcf1^{hi} CD8$^+$ T Cells

(A–H) B6 *Tcf7*^{GFP} mice were vaccinated as indicated with a modified Ovalbumin peptide and Pam3CSK4 in Montanide (Ova) or with Pam3CSK4 in Montanide (Ø).

(B, C, and E) Abundance and (D and F) *Tcf7*^{GFP} and CD62L expression by K^{b}Ova$^+$ CD8$^+$ T cells in the blood on d21 and d35 (B–D) and in the spleen on d35 post-vaccination (E–G). (H) IL-2 and TNF-α production by d35 splenic IFN-γ$^+$ cells.

(I–K) Healthy volunteers received a yellow fever vaccine, and peripheral blood CD8$^+$ T cells were analyzed 14 days later. (I) TCF1 expression by A2/LLW tetramer$^+$ CD8$^+$ T cells (left) and expression of CCR7, CD45RA and CD95 by TCF1^{hi} and TCF1^{lo} A2/LLW$^+$ cells (right). (J) Frequencies of A2/LLW$^+$ TCF1^{hi} or TCF1^{lo} cells among CD8$^+$ T cells. (K) Presence of CCR7, CD45RA, and CD95-defined subsets among A2/LLW$^+$ TCF1^{hi} and TCF1^{lo} cells.

Data in (B–G) are pooled from 2 experiments with 9–10 mice per group or (H) are representative of 2 experiments with n = 4 mice. Data in (J and K) are from 6 healthy donors analyzed using 2 staining panels (see STAR Methods). Total naive and CCR7$^-$ CD8$^+$ T cells were used as reference for gating TCF1^{hi} cells. Mean ± SD are shown. Statistics: (C) one-way ANOVA with Tukey's test; (D–H) non-paired t test; (J) intra-individual pairing, Wilcoxon test, and (K) adjusted p values from Sidak's multiple comparisons test with *p < 0.05; **p < 0.01; ***p < 0.001; ****p < 0.0001; and (ns) p > 0.05.

comparable (Figure 6D). Furthermore, the recall expansion of *Tcf7*$^{-/-}$ *Tcf7*^{GFPhi} cells was compromised (Figure 6E), and secondary *Tcf7*$^{-/-}$ *Tcf7*^{GFPhi} cells were essentially absent (Figures 6F and 6G). It was conceivable that some of the observed phenotypes were secondary to impaired T cell development in *Tcf7*$^{-/-}$ mice (Verbeek et al., 1995). However, this was unlikely, as *Tcf7* silencing in naive WT P14 cells produced comparable effects (see below). Tcf1 expression thus ensured the stem-cell-like
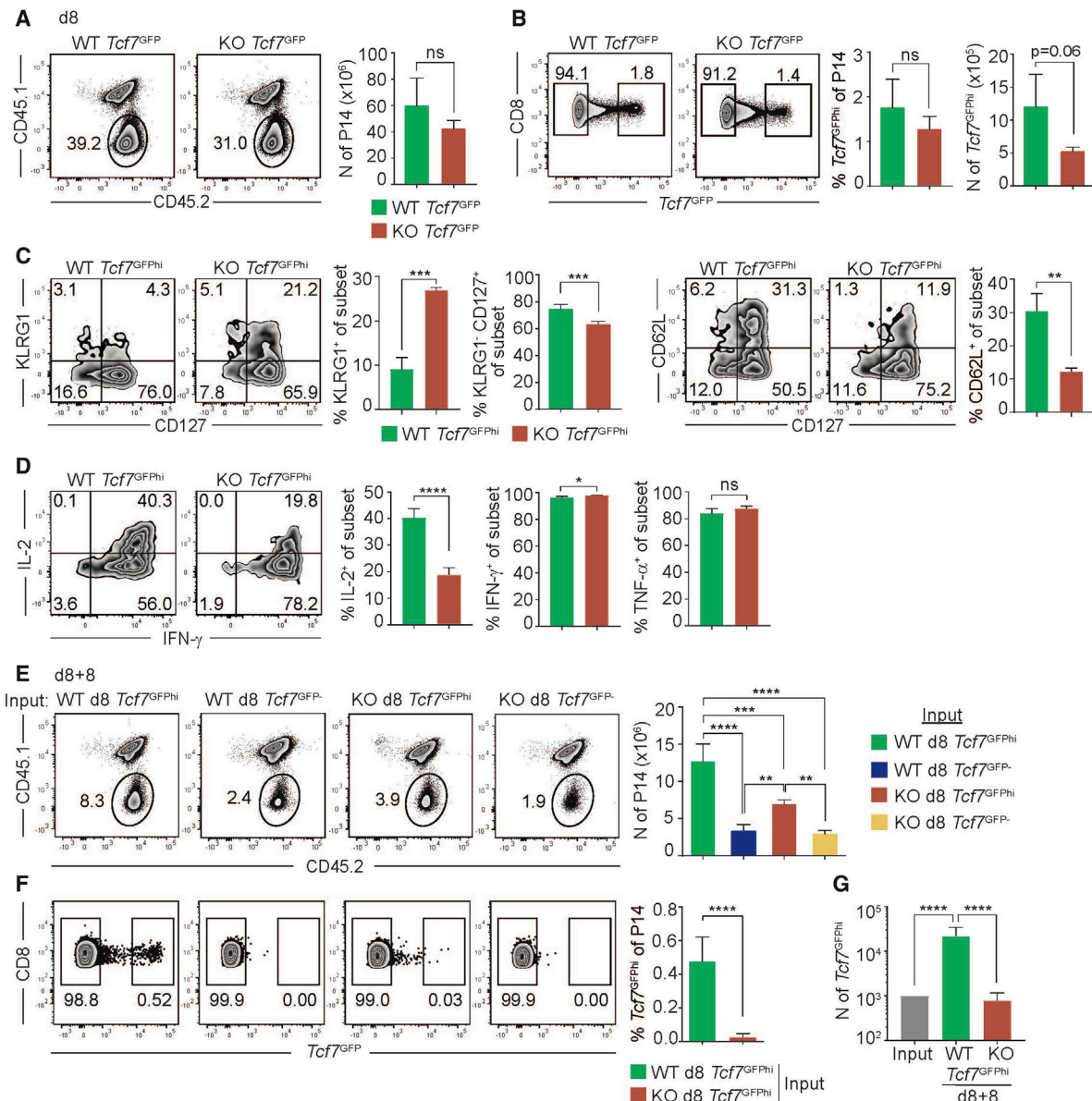
Figure 6. Tcf1 Is Essential for the Stemness of d8 *Tcf7*^{GFPhi} CD8⁺ T Cells

(A–D) B6 mice (CD45.1/2) were transplanted with WT or *Tcf7*⁻/⁻ (KO) *Tcf7*^{GFP} P14 cells (CD45.2) and infected with LCMV WE. (A) Abundance of P14 cells in the spleen at d8 p.i. and (B) expression of *Tcf7*^{GFP}. Phenotype (C) and cytokine production (D) by WT and KO *Tcf7*^{GFPhi} P14 cells.

(E–G) Recall response of sorted d8 WT and KO *Tcf7*^{GFPhi} P14 cells. (E) Abundance of P14 cells in the spleen and (F) *Tcf7*^{GFP} expression 8 days later (d8+8). (G) Abundance of secondary *Tcf7*^{GFPhi} cells compared to input.

Data are representative of 3 experiments with 4 mice per group (A–C), representative of 2 experiments with 5–6 mice per group (D), or compiled from 2 experiments with 5–7 mice per group (E–G). Mean ± SD are shown. Statistics: non-paired t test (A–D and F) or one-way ANOVA with Tukey's test (E and G) with *p < 0.05; **p < 0.01; ***p < 0.001; ****p < 0.0001; and (ns) p > 0.05. See also Figure S7.

properties of effector-phase *Tcf7*^{GFPhi} cells by counteracting their differentiation and preserving their recall expansion and self-renewal capacity.

Tcf1-Dependent Genes Ensure Stemness of Effector-Phase *Tcf7*^{GFPhi} CD8⁺ T Cells

We next aimed at identifying Tcf1-dependent genes that ensured the stemness of effector-phase *Tcf7*^{GFPhi} CD8⁺ T cells. The transcriptomes of WT and *Tcf7*⁻/⁻ d8 *Tcf7*^{GFPhi} cells differed consid-

erably both based on PCA (Figure 7A) and the number of differentially expressed genes (DEG) (n = 607, FDR < 5%, FC > 2) (Figure 7B) (Table S4). By comparison, the corresponding d8 *Tcf7*^{GFP-} populations overlapped in the PCA and had few DEG (n = 72) (Figure 7A) (Table S4). *Tcf7*⁻/⁻ d8 *Tcf7*^{GFPhi} cells overexpressed multiple effector genes and were enriched in an IL-2-STAT5 signaling signature (FDR = 0.01) (Figures S7C and S7D), confirming that Tcf1 counteracted the differentiation of effector-phase *Tcf7*^{GFPhi} cells. On the other hand, the
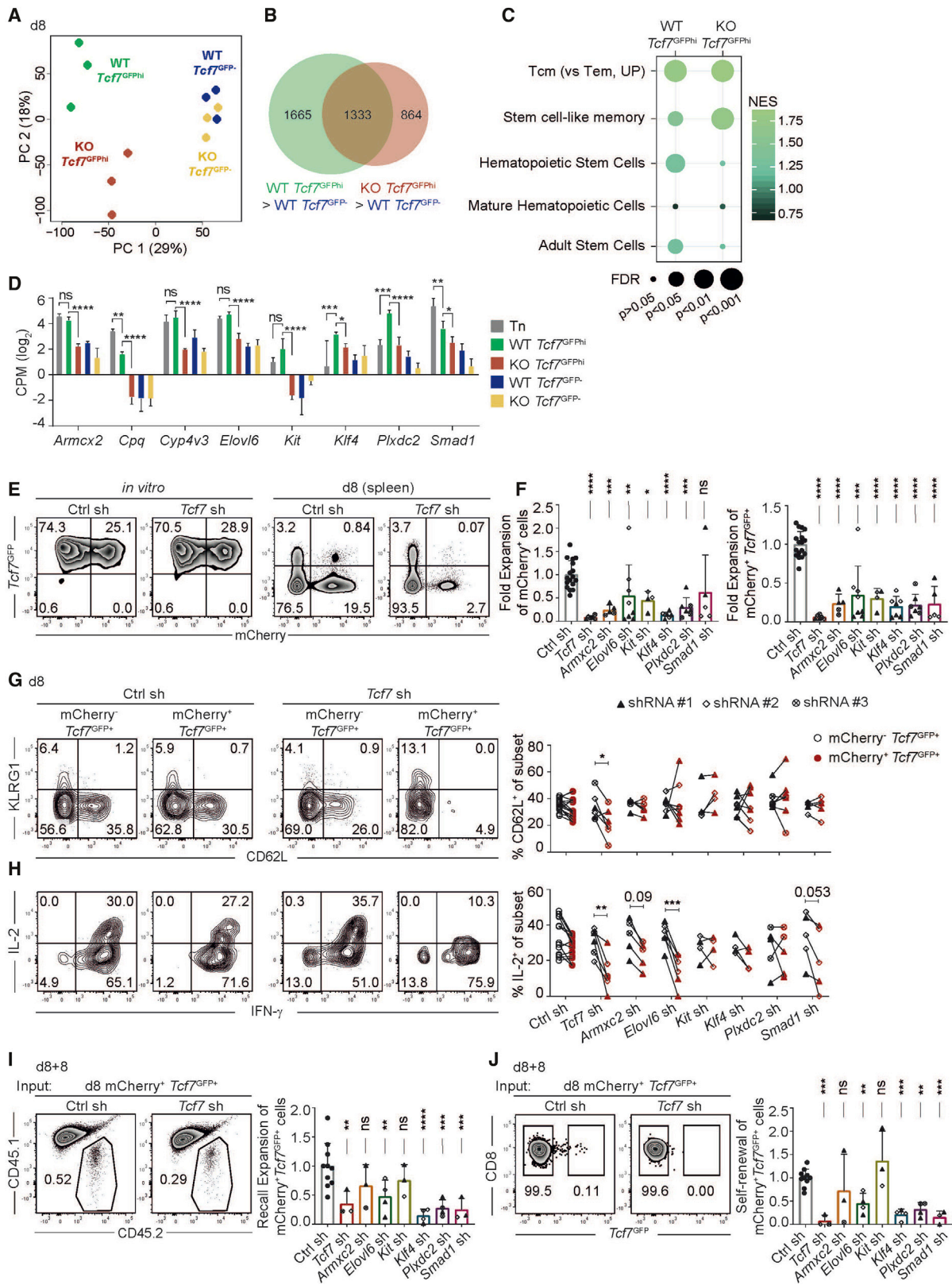
(legend on next page)

transcriptome of $Tcf7^{-/-}$ $Tcf7^{GFPhi}$ cells no longer overlapped with the hematopoietic and the adult stem-cell signatures (Ivanova et al., 2002) (Wong et al., 2008) (Figure 7C). In contrast, the overlaps with the Tcm (Mackay et al., 2016) and the alternative stem-cell-like memory signature (Pace et al., 2018) were not affected (Figure 7C), and the expression of the central memory genes *Bcl6, Foxo1, Id3, Myb*, and *Stat3* was not altered (Figure S7E). Impaired stemness of $Tcf7^{-/-}$ d8 $Tcf7^{GFPhi}$ cells thus correlated with reduced expression of adult stem-cell genes. Hematopoietic stem and progenitor cells (n = 517 genes) (Ivanova et al., 2002), adult stem cells (n = 494) (Wong et al., 2008), and WT d8 $Tcf7^{GFPhi}$ cells (n = 602) (Table S1) shared 18 genes, 8 of which were reduced in $Tcf7^{-/-}$ compared to WT d8 $Tcf7^{GFPhi}$ cells (Log$_2$FC > 1, p < 0.05) (Figure 7D). The TSS of 6 of the 8 genes was more accessible in d8 $Tcf7^{GFPhi}$ compared to d8 $Tcf7^{GFP-}$ cells (Figures S7F and S7G) (Table S3), suggesting that the downregulation of these genes during differentiation was epigenetically regulated. The remaining 2 genes (*Elovl6, Klf4*) were bound by Tcf1 in naive CD8+ T cells (Figure S7H) based on published ChIPseq data (Xing et al., 2016), indicating Tcf1-dependent transcriptional regulation.

To test the importance of Tcf1-dependent genes for CD8+ T cell stemness, we mimicked the reduced gene expression observed in $Tcf7^{-/-}$ d8 $Tcf7^{GFPhi}$ cells using lentivirus-based short-hairpin (sh) RNA constructs. We confirmed reduced target-gene expression in transduced (mCherry+) $Tcf7^{DTR-GFP}$ (hereafter referred to as $Tcf7^{GFP}$) P14 cells *in vitro* or at d8 post-LCMV infection (Figures S7I–S7L). Following transduction *in vitro*, $Tcf7^{GFP}$ P14 cells (CD45.2) were transplanted into B6 recipient mice (CD45.1) that had been infected with LCMV one day earlier. At d8 p.i., *Tcf7* sh reduced the abundance of $Tcf7^{GFP+}$ mCherry+ cells 16-fold compared to a scrambled control (Ctrl) sh construct (Figures 7E and 7F). Residual d8 $Tcf7^{GFP+}$ *Tcf7* sh (mCherry+) cells showed evidence of differentiation based on increased KLRG1 and decreased CD62L and IL-2 expression (Figure 7G, 7H, and S7M). Furthermore, *Tcf7* sh impaired the recall expansion and the self-renewal of d8 $Tcf7^{GFP+}$ mCherry+ cells (Figures 7I and 7J). These data confirmed and extended the results obtained with $Tcf7^{-/-}$ $Tcf7^{GFPhi}$ cells (Figures 6A–6G) and validated our approach to functionally test the role of adult stem-cell genes for CD8+ T cell stemness.

Similar to *Tcf7* sh, silencing of each of the 6 adult stem-cell genes reduced the generation of d8 $Tcf7^{GFP+}$ cells (Figure 7F). *Elovl6* and *Smad1* shRNA also reduced IL-2 and increased KLRG1 expression but, unlike *Tcf7* sh, did not reduce CD62L

expression (Figures 7G and S7M). Finally, *Klf4, Elovl6, Plxdc2*, and *Smad1* silencing reduced the recall expansion and the self-renewal of d8 $Tcf7^{GFP+}$ cells (Figures 7I and 7J). These experiments thus identified a set of Tcf1-dependent genes essential for CD8+ T cell stemness.

DISCUSSION

A prevalent view of CD8+ T cell differentiation is that some MP cells differentiate into Tcm cells following antigen clearance. As MP cells have cytotoxic activity and mostly lack central memory features such as CD62L expression (Bannard et al., 2009; Joshi et al., 2007; Youngblood et al., 2017), formation of Tcm cells is thought to involve the de-differentiation of cytolytic effector cells. However, here we identified effector-phase cells expressing high amounts of *Tcf7* that represented a small subset of MP cells, many of which expressed CD62L and that lacked evidence of cytolytic differentiation. These cells may correspond to CD62L+ effector cells previously observed in bacterial (L.m.) and viral (VSV) infection (Obar and Lefrançois, 2010). While prior (Lin et al., 2016) and our own cell transfers suggested that effector-stage $Tcf7^{hi}$ cells predominantly yield Tcm cells, our lineage tracing and ablation experiments established that central memory quantitatively and almost exclusively derived from effector-stage $Tcf7^{hi}$ cells (referred to hereafter as Tpcm). Further, Tpcm cells already displayed key functions associated with central memory cells, suggesting that central memory did not emerge after pathogen clearance. Consequently, the findings suggested that primed Tn cells expand and generate Tpcm cells that quantitatively yield Tcm cells and whose further stimulation produces cytolytic effector cells. This scenario is consistent with the predominant central memory formation in response to dendritic cell vaccination in the absence of systemic inflammation (Pham et al., 2009) and with recent findings regarding T cell differentiation in persistent viral infections and cancer. The latter responses are sustained by a $Tcf7^{hi}$ PD-1+ CD8+ T cell subpopulation (memory-like [Tml] cells), which lacks evidence of cytolytic effector differentiation but continuously yields differentiated cells with cytolytic potential, while reproducing itself (Im et al., 2016; Jadhav et al., 2019; Miller et al., 2019; Siddiqui et al., 2019; Utzschneider et al., 2016). Despite considerable phenotypic and functional differences between Tml and Tpcm cells, the data suggest that cytolytic effector cells derive from less differentiated CD8+ T cells with stem-cell-like properties in response to both acute as well as chronic stimulation.

Figure 7. Tcf1-Dependent Genes Are Essential for CD8+ T Cell Stemness
(A–D) Sorted d8 WT and $Tcf7^{-/-}$ (KO) $Tcf7^{GFPhi}$ and $Tcf7^{GFP-}$ P14 cells (CD45.2) were subjected to transcriptome analysis. (A) PCA of the indicated populations of cells. Each dot represents a biological replicate. (B) Genes differentially expressed between WT and KO $Tcf7^{GFPhi}$ cells, each relative to WT $Tcf7^{GFP-}$ cells. (C) GSEA of WT and KO $Tcf7^{GFPhi}$ cells (each versus WT $Tcf7^{GFP-}$ cells) relative to the indicated gene signatures. Dot sizes and colors indicate the FDR and the NES, respectively. (D) Expression of adult stem-cell genes in the indicated population of cells. Log2 CPM (counts per million). (E–G) P14 $Tcf7^{GFP}$ cells were transduced with gene-specific Lentiviral sh RNA constructs or a scrambled control (Ctrl).
(E) Expression of sh constructs (mCherry+) by $Tcf7^{GFP}$ P14 cells *in vitro* (left) and following the response to LCMV *in vivo* (right).
(F–H) D8 p.i. P14 cells were analyzed for the abundance of mCherry+ (left) and of mCherry+ $Tcf7^{GFP+}$ P14 cells (right) both relative to input and normalized to the Ctrl sh (=1.0). Gated mCherry− and mCherry+ $Tcf7^{GFP+}$ P14 cells were analyzed for (G) CD62L and KLRG1 expression and (H) IL-2 and IFN-γ production.
(I and J) Recall response of sorted d8 mCherry+ $Tcf7^{GFP+}$ P14 cells. (I) Abundance of mCherry+ P14 cells and of (J) mCherry+ $Tcf7^{GFP+}$ P14 cells 8 days later (d8 + 8). Data in (I) and (J) are normalized to the Ctrl sh (=1.0).
Data in (E–J) involve at least 2 independent experiments with a total of 4–15 mice per gene and at least 2 distinct sh constructs per gene (one for the Ctrl sh). Means ± SD are shown. Statistics: two-way ANOVA with Tukey's test (D); one-Way ANOVA with Fisher's LSD test (F, I, and J); or two-way ANOVA with Fisher's LSD test (G and H) with *p < 0.05; **p < 0.01; ***p < 0.001; ****p < 0.0001; and (ns) p > 0.05. See also Figure S7.

The absence of Tcf1 protein increased the differentiation of Tpcm cells and reduced their recall expansion and self-renewal capacity. While increased differentiation of $Tcf7^{-/-}$ CD8$^+$ T cells responding to infection (Boudousquié et al., 2014; Jeannet et al., 2010; Tiemessen et al., 2014; Wu et al., 2016; Zhou et al., 2010) or vaccination (Danilo et al., 2018) has been noted before, it is important to point out that the role of Tcf1 in the stem-like $Tcf7^{hi}$ CD8$^+$ T cell subset has not been addressed before. While the absence or the epigenetic silencing of $Tcf7$ and other memory transcription factors in effector cells is necessary for full effector differentiation (Danilo et al., 2018; Gray et al., 2017; Ladle et al., 2016; Pace et al., 2018; Youngblood et al., 2017), we identified and functionally tested Tcf1-dependent genes that are expressed in Tpcm cells and adult stem cells and that are essential in CD8$^+$ T cell stemness. While $Klf4$ is a pluripotency factor necessary to reprogram differentiated adult cells to an embryonic-like state (Takahashi and Yamanaka, 2006), the role of the remaining genes for CD8$^+$ T cell stemness remains to be elucidated. The downregulation of most adult stem-cell genes in $Tcf7^-$ cells was associated with reduced accessibility of their TSS, suggesting stable repression of the stemness program in Teff cells.

The identification of effector-stage CD8$^+$ T cells with central memory function has implications for T cell vaccination and further types of therapeutic interventions targeting T cells. The abundance and the properties of such cells can now be assessed early during a primary response, which should greatly facilitate the optimization of the generation or maintenance of Tcm cells.

STAR★METHODS

Detailed methods are provided in the online version of this paper and include the following:

- KEY RESOURCES TABLE
- RESOURCE AVAILABILITY
  - Lead Contact
  - Materials Availability
  - Data and Code Availability
- EXPERIMENTAL MODEL AND SUBJECT DETAILS
  - Mice
  - Human vaccination study
- METHOD DETAILS
  - LCMV infections
  - Adoptive T cell transfer
  - Tamoxifen (TAM) and diphtheria toxin (DT) treatment
  - Vaccination
  - Plasmids, lentiviral vectors, virus production and T cell transduction
  - *In vitro* killing assay
  - Tissue preparation and cell suspensions
  - Flow cytometry and cell sorting
  - Immunofluorescence labeling and microscopy
  - Image analysis and cellular identification
  - RT-qPCR analysis
  - RNA-seq analysis
  - ATAC-seq analysis
  - Human peripheral blood collection and analysis
- QUANTIFICATION AND STATISTICAL ANALYSIS

AUTHOR CONTRIBUTIONS

D.P.F. designed and performed most experiments and prepared figures; J.G.S. performed lineage tracing; and M.C. performed the virus control experiment. T.W. and M.D. performed bioinformatics analysis; S.A.F.M. and D.S. performed the yellow fever vaccination and analysis; L.S. and S.A.L. performed immunofluorescence staining and analysis; R.M. and J.A.J. supported the quantitative image analysis; L.T. provided reagents for vaccination; I.S. provided critical mouse strain; and W.H. conceived and supervised study and wrote the paper.

DECLARATION OF INTERESTS

The authors declare no competing interests.

REFERENCES

Anders, S., Pyl, P.T., and Huber, W. (2015). HTSeq–a Python framework to work with high-throughput sequencing data. Bioinformatics *31*, 166–169.

Bannard, O., Kraman, M., and Fearon, D.T. (2009). Secondary replicative function of CD8+ T cells that had developed an effector phenotype. Science *323*, 505–509.

Battegay, M., Cooper, S., Althage, A., Bänziger, J., Hengartner, H., and Zinkernagel, R.M. (1991). Quantification of lymphocytic choriomeningitis virus with an immunological focus assay in 24- or 96-well plates. J. Virol. Methods *33*, 191–198.

Benjamini, Y., and Hochberg, Y. (1995). Controlling the false discovery rate: a practical and powerful approach to multiple testing. J. R. Stat. Soc. B *57*, 289–300.

Blattman, J.N., Antia, R., Sourdive, D.J., Wang, X., Kaech, S.M., Murali-Krishna, K., Altman, J.D., and Ahmed, R. (2002). Estimating the precursor frequency of naive antigen-specific CD8 T cells. J. Exp. Med. *195*, 657–664.

Boudousquié, C., Danilo, M., Pousse, L., Jeevan-Raj, B., Angelov, G.S., Chennupati, V., Zehn, D., and Held, W. (2014). Differences in the transduction of canonical Wnt signals demarcate effector and memory CD8 T cells with distinct recall proliferation capacity. J. Immunol. *193*, 2784–2791.

Buenrostro, J.D., Wu, B., Chang, H.Y., and Greenleaf, W.J. (2015). ATAC-seq: A Method for Assaying Chromatin Accessibility Genome-Wide. Curr Protoc Mol Biol *109*, 21–29.

Chang, J.T., Palanivel, V.R., Kinjyo, I., Schambach, F., Intlekofer, A.M., Banerjee, A., Longworth, S.A., Vinup, K.E., Mrass, P., Oliaro, J., et al. (2007). Asymmetric T lymphocyte division in the initiation of adaptive immune responses. Science *315*, 1687–1691.

Cui, W., Joshi, N.S., Jiang, A., and Kaech, S.M. (2009). Effects of Signal 3 during CD8 T cell priming: Bystander production of IL-12 enhances effector T cell expansion but promotes terminal differentiation. Vaccine 27, 2177–2187.

Cui, W., Liu, Y., Weinstein, J.S., Craft, J., and Kaech, S.M. (2011). An interleukin-21-interleukin-10-STAT3 pathway is critical for functional maturation of memory CD8+ T cells. Immunity 35, 792–805.

Danilo, M., Chennupati, V., Silva, J.G., Siegert, S., and Held, W. (2018). Suppression of Tcf1 by inflammatory cytokines facilitates effector CD8 T cell differentiation. Cell Rep. 22, 2107–2117.

Davis, MPA, van Dongen, S., Abreu-Goodger, C., Bartonicek, N., and Enright, A.J. (2013). Kraken: a set of tools for quality control and analysis of high-throughput sequence data. Methods 63, 41–49.

Dillon, S.R., Jameson, S.C., and Fink, P.J. (1994). V beta 5+ T cell receptors skew toward OVA+H-2Kb recognition. J. Immunol. 152, 1790–1801.

Dobin, A., Davis, C.A., Schlesinger, F., Drenkow, J., Zaleski, C., Jha, S., Batut, P., Chaisson, M., and Gingeras, T.R. (2013). STAR: ultrafast universal RNA-seq aligner. Bioinformatics 29, 15–21.

Durinck, S., Spellman, P.T., Birney, E., and Huber, W. (2009). Mapping identifiers for the integration of genomic datasets with the R/Bioconductor package biomaRt. Nat. Protoc. 4, 1184–1191.

Gattinoni, L., Lugli, E., Ji, Y., Pos, Z., Paulos, C.M., Quigley, M.F., Almeida, J.R., Gostick, E., Yu, Z., Carpenito, C., et al. (2011). A human memory T cell subset with stem cell-like properties. Nat. Med. 17, 1290–1297.

Gautam, S., Fioravanti, J., Zhu, W., Le Gall, J.B., Brohawn, P., Lacey, N.E., Hu, J., Hocker, J.D., Hawk, N.V., Kapoor, V., et al. (2019). The transcription factor c-Myb regulates CD8+ T cell stemness and antitumor immunity. Nat. Immunol. 20, 337–349.

Graef, P., Buchholz, V.R., Stemberger, C., Flossdorf, M., Henkel, L., Schiemann, M., Drexler, I., Höfer, T., Riddell, S.R., and Busch, D.H. (2014). Serial transfer of single-cell-derived immunocompetence reveals stemness of CD8(+) central memory T cells. Immunity 41, 116–126.

Gray, S.M., Amezquita, R.A., Guan, T., Kleinstein, S.H., and Kaech, S.M. (2017). Polycomb Repressive Complex 2-Mediated Chromatin Repression Guides Effector CD8+ T Cell Terminal Differentiation and Loss of Multipotency. Immunity 46, 596–608.

Gu, Z., Eils, R., and Schlesner, M. (2016). Complex heatmaps reveal patterns and correlations in multidimensional genomic data. Bioinformatics 32, 2847–2849.

Gullicksrud, J.A., Li, F., Xing, S., Zeng, Z., Peng, W., Badovinac, V.P., Harty, J.T., and Xue, H.H. (2017). Differential Requirements for Tcf1 Long Isoforms in CD8+ and CD4+ T Cell Responses to Acute Viral Infection. J. Immunol. 199, 911–919.

Henning, A.N., Roychoudhuri, R., and Restifo, N.P. (2018). Epigenetic control of CD8+ T cell differentiation. Nat. Rev. Immunol. 18, 340–356.

Hess Michelini, R., Doedens, A.L., Goldrath, A.W., and Hedrick, S.M. (2013). Differentiation of CD8 memory T cells depends on Foxo1. J. Exp. Med. 210, 1189–1200.

Im, S.J., Hashimoto, M., Gerner, M.Y., Lee, J., Kissick, H.T., Burger, M.C., Shan, Q., Hale, J.S., Lee, J., Nasti, T.H., et al. (2016). Defining CD8+ T cells that provide the proliferative burst after PD-1 therapy. Nature 537, 417–421.

Ivanova, N.B., Dimos, J.T., Schaniel, C., Hackney, J.A., Moore, K.A., and Lemischka, I.R. (2002). A stem cell molecular signature. Science 298, 601–604.

Jadhav, R.R., Im, S.J., Hu, B., Hashimoto, M., Li, P., Lin, J.X., Leonard, W.J., Greenleaf, W.J., Ahmed, R., and Goronzy, J.J. (2019). Epigenetic signature of PD-1+ TCF1+ CD8 T cells that act as resource cells during chronic viral infection and respond to PD-1 blockade. Proc. Natl. Acad. Sci. USA 116, 14113–14118.

Jeannet, G., Boudousquié, C., Gardiol, N., Kang, J., Huelsken, J., and Held, W. (2010). Essential role of the Wnt pathway effector Tcf-1 for the establishment of functional CD8 T cell memory. Proc. Natl. Acad. Sci. USA 107, 9777–9782.

Ji, Y., Pos, Z., Rao, M., Klebanoff, C.A., Yu, Z., Sukumar, M., Reger, R.N., Palmer, D.C., Borman, Z.A., Muranski, P., et al. (2011). Repression of the DNA-binding inhibitor Id3 by Blimp-1 limits the formation of memory CD8+ T cells. Nat. Immunol. 12, 1230–1237.

Joshi, N.S., Cui, W., Chandele, A., Lee, H.K., Urso, D.R., Hagman, J., Gapin, L., and Kaech, S.M. (2007). Inflammation directs memory precursor and short-lived effector CD8(+) T cell fates via the graded expression of T-bet transcription factor. Immunity 27, 281–295.

Kaech, S.M., and Cui, W. (2012). Transcriptional control of effector and memory CD8+ T cell differentiation. Nat. Rev. Immunol. 12, 749–761.

Kaech, S.M., Hemby, S., Kersh, E., and Ahmed, R. (2002). Molecular and functional profiling of memory CD8 T cell differentiation. Cell 111, 837–851.

Kakaradov, B., Arsenio, J., Widjaja, C.E., He, Z., Aigner, S., Metz, P.J., Yu, B., Wehrens, E.J., Lopez, J., Kim, S.H., et al. (2017). Early transcriptional and epigenetic regulation of CD8+ T cell differentiation revealed by single-cell RNA sequencing. Nat. Immunol. 18, 422–432.

Kim, M.V., Ouyang, W., Liao, W., Zhang, M.Q., and Li, M.O. (2013). The transcription factor Foxo1 controls central-memory CD8+ T cell responses to infection. Immunity 39, 286–297.

Klebanoff, C.A., Gattinoni, L., Torabi-Parizi, P., Kerstann, K., Cardones, A.R., Finkelstein, S.E., Palmer, D.C., Antony, P.A., Hwang, S.T., Rosenberg, S.A., et al. (2005). Central memory self/tumor-reactive CD8+ T cells confer superior antitumor immunity compared with effector memory T cells. Proc. Natl. Acad. Sci. USA 102, 9571–9576.

Ladle, B.H., Li, K.P., Phillips, M.J., Pucsek, A.B., Haile, A., Powell, J.D., Jaffee, E.M., Hildeman, D.A., and Gamper, C.J. (2016). De novo DNA methylation by DNA methyltransferase 3a controls early effector CD8+ T-cell fate decisions following activation. Proc. Natl. Acad. Sci. USA 113, 10631–10636.

Li, H., Handsaker, B., Wysoker, A., Fennell, T., Ruan, J., Homer, N., Marth, G., Abecasis, G., and Durbin, R.; 1000 Genome Project Data Processing Subgroup (2009). The Sequence Alignment/Map format and SAMtools. Bioinformatics 25, 2078–2079.

Liberzon, A., Birger, C., Thorvaldsdóttir, H., Ghandi, M., Mesirov, J.P., and Tamayo, P. (2015). The Molecular Signatures Database (MSigDB) hallmark gene set collection. Cell Syst. 1, 417–425.

Lin, W.W., Nish, S.A., Yen, B., Chen, Y.-H., Adams, W.C., Kratchmarov, R., Rothman, N.J., Bhandoola, A., Xue, H.-H., and Reiner, S.L. (2016). CD8+ T Lymphocyte Self-Renewal during Effector Cell Determination. Cell Rep. 17, 1773–1782.

Mackay, L.K., Minnich, M., Kragten, N.A.M., Liao, Y., Nota, B., Seillet, C., Zaid, A., Man, K., Preston, S., Freestone, D., et al. (2016). Hobit and Blimp1 instruct a universal transcriptional program of tissue residency in lymphocytes. Science 352, 459–463.

Martin, M.T., Knudsen, T.B., Reif, D.M., Houck, K.A., Judson, R.S., Kavlock, R.J., and Dix, D.J. (2011). Predictive model of rat reproductive toxicity from ToxCast high throughput screening. Biol. Reprod. 85, 327–339.

Miller, B.C., Sen, D.R., Al Abosy, R., Bi, K., Virkud, Y.V., LaFleur, M.W., Yates, K.B., Lako, A., Felt, K., Naik, G.S., et al. (2019). Subsets of exhausted CD8+ T cells differentially mediate tumor control and respond to checkpoint blockade. Nat. Immunol. 20, 326–336.

Obar, J.J., and Lefrançois, L. (2010). Early signals during CD8 T cell priming regulate the generation of central memory cells. J. Immunol. 185, 263–272.

Pace, L., Goudot, C., Zueva, E., Gueguen, P., Burgdorf, N., Waterfall, J.J., Quivy, J.P., Almouzni, G., and Amigorena, S. (2018). The epigenetic control of stemness in CD8+ T cell fate commitment. Science 359, 177–186.

Pham, N.L., Badovinac, V.P., and Harty, J.T. (2009). A default pathway of memory CD8 T cell differentiation after dendritic cell immunization is deflected by encounter with inflammatory cytokines during antigen-driven proliferation. J. Immunol. 183, 2337–2348.

Pircher, H., Mak, T.W., Lang, R., Ballhausen, W., Rüedi, E., Hengartner, H., Zinkernagel, R.M., and Bürki, K. (1989). T cell tolerance to Mlsa encoded antigens in T cell receptor V beta 8.1 chain transgenic mice. EMBO J. 8, 719–727.

Ramírez, F., Dündar, F., Diehl, S., Grüning, B.A., and Manke, T. (2014). deepTools: a flexible platform for exploring deep-sequencing data. Nucleic Acids Res. 42, W187–W191.

Restifo, N.P., and Gattinoni, L. (2013). Lineage relationship of effector and memory T cells. Curr. Opin. Immunol. 25, 556–563.

Ritchie, M.E., Phipson, B., Wu, D., Hu, Y., Law, C.W., Shi, W., and Smyth, G.K. (2015). limma powers differential expression analyses for RNA-sequencing and microarray studies. Nucleic Acids Res. *43*, e47.

Robinson, M.D., McCarthy, D.J., and Smyth, G.K. (2010). edgeR: a Bioconductor package for differential expression analysis of digital gene expression data. Bioinformatics *26*, 139–140.

Robinson, J.T., Thorvaldsdóttir, H., Winckler, W., Guttman, M., Lander, E.S., Getz, G., and Mesirov, J.P. (2011). Integrative genomics viewer. Nat. Biotechnol. *29*, 24–26.

Scott-Browne, J.P., López-Moyado, I.F., Trifari, S., Wong, V., Chavez, L., Rao, A., and Pereira, R.M. (2016). Dynamic Changes in Chromatin Accessibility Occur in CD8⁺ T Cells Responding to Viral Infection. Immunity *45*, 1327–1340.

Siddiqui, I., Schaeuble, K., Chennupati, V., Fuertes Marraco, S.A., Calderon-Copete, S., Pais Ferreira, D., Carmona, S.J., Scarpellino, L., Gfeller, D., Pradervand, S., et al. (2019). Intratumoral Tcf1(+)PD-1(+)CD8(+) T Cells with Stem-like Properties Promote Tumor Control in Response to Vaccination and Checkpoint Blockade Immunotherapy. Immunity *50*, 195–211.e110.

Snippert, H.J., van der Flier, L.G., Sato, T., van Es, J.H., van den Born, M., Kroon-Veenboer, C., Barker, N., Klein, A.M., van Rheenen, J., Simons, B.D., and Clevers, H. (2010). Intestinal crypt homeostasis results from neutral competition between symmetrically dividing Lgr5 stem cells. Cell *143*, 134–144.

Subramanian, A., Tamayo, P., Mootha, V.K., Mukherjee, S., Ebert, B.L., Gillette, M.A., Paulovich, A., Pomeroy, S.L., Golub, T.R., Lander, E.S., and Mesirov, J.P. (2005). Gene set enrichment analysis: a knowledge-based approach for interpreting genome-wide expression profiles. Proc. Natl. Acad. Sci. USA *102*, 15545–15550.

Takahashi, K., and Yamanaka, S. (2006). Induction of pluripotent stem cells from mouse embryonic and adult fibroblast cultures by defined factors. Cell *126*, 663–676.

Tiemessen, M.M., Baert, M.R.M., Kok, L., van Eggermond, M.C.J.A., van den Elsen, P.J., Arens, R., and Staal, F.J.T. (2014). T Cell factor 1 represses CD8+ effector T cell formation and function. Journal of immunology (Baltimore, Md: 1950) *193*, 5480–5487.

Utzschneider, D.T., Charmoy, M., Chennupati, V., Pousse, L., Ferreira, D.P., Calderon-Copete, S., Danilo, M., Alfei, F., Hofmann, M., Wieland, D., et al. (2016). T Cell Factor 1-Expressing Memory-like CD8(+) T Cells Sustain the Immune Response to Chronic Viral Infections. Immunity *45*, 415–427.

Verbeek, S., Izon, D., Hofhuis, F., Robanus-Maandag, E., te Riele, H., van de Wetering, M., Oosterwegel, M., Wilson, A., MacDonald, H.R., and Clevers, H. (1995). An HMG-box-containing T-cell factor required for thymocyte differentiation. Nature *374*, 70–74.

Wang, L., Wang, S., and Li, W. (2012). RSeQC: quality control of RNA-seq experiments. Bioinformatics *28*, 2184–2185.

Wang, D., Diao, H., Getzler, A.J., Rogal, W., Frederick, M.A., Milner, J., Yu, B., Crotty, S., Goldrath, A.W., and Pipkin, M.E. (2018). The Transcription Factor Runx3 Establishes Chromatin Accessibility of cis-Regulatory Landscapes that Drive Memory Cytotoxic T Lymphocyte Formation. Immunity *48*, 659–674.e656.

West, E.E., Youngblood, B., Tan, W.G., Jin, H.-T., Araki, K., Alexe, G., Konieczny, B.T., Calpe, S., Freeman, G.J., Terhorst, C., et al. (2011). Tight regulation of memory CD8(+) T cells limits their effectiveness during sustained high viral load. Immunity *35*, 285–298.

Wong, D.J., Liu, H., Ridky, T.W., Cassarino, D., Segal, E., and Chang, H.Y. (2008). Module map of stem cell genes guides creation of epithelial cancer stem cells. Cell Stem Cell *2*, 333–344.

Wu, T., Ji, Y., Moseman, E.A., Xu, H.C., Manglani, M., Kirby, M., Anderson, S.M., Handon, R., Kenyon, E., Elkahloun, A., et al. (2016). The TCF1-Bcl6 axis counteracts type I interferon to repress exhaustion and maintain T cell stemness. Sci. Immunol. *1*, eaai8593.

Xing, S., Li, F., Zeng, Z., Zhao, Y., Yu, S., Shan, Q., Li, Y., Phillips, F.C., Maina, P.K., Qi, H.H., et al. (2016). Tcf1 and Lef1 transcription factors establish CD8(+) T cell identity through intrinsic HDAC activity. Nat. Immunol. *17*, 695–703.

Youngblood, B., Hale, J.S., Kissick, H.T., Ahn, E., Xu, X., Wieland, A., Araki, K., West, E.E., Ghoneim, H.E., Fan, Y., et al. (2017). Effector CD8 T cells dedifferentiate into long-lived memory cells. Nature *552*, 404–409.

Zhang, Y., Liu, T., Meyer, C.A., Eeckhoute, J., Johnson, D.S., Bernstein, B.E., Nusbaum, C., Myers, R.M., Brown, M., Li, W., and Liu, X.S. (2008). Model-based analysis of ChIP-Seq (MACS). Genome Biol. *9*, R137.

Zhao, D.M., Yu, S., Zhou, X., Haring, J.S., Held, W., Badovinac, V.P., Harty, J.T., and Xue, H.H. (2010). Constitutive activation of Wnt signaling favors generation of memory CD8 T cells. J. Immunol. *184*, 1191–1199.

Zhou, X., Yu, S., Zhao, D.M., Harty, J.T., Badovinac, V.P., and Xue, H.H. (2010). Differentiation and persistence of memory CD8(+) T cells depend on T cell factor 1. Immunity *33*, 229–240.

STAR★METHODS

KEY RESOURCES TABLE

REAGENT or RESOURCE	SOURCE	IDENTIFIER
Antibodies		
Anti-Mouse CD4 – AF700	eBioscience	Clone GK1.5; RRID:AB_493999
Anti-Mouse CD8α – PerCP-Cy5.5, PE Cy7, APC-eF780 or BV 650	eBioscience / BioLegend	Clone 53.6.7; RRID:AB_1107004 RRID:AB_469583 RRID:AB_1272185 RRID:AB_2563056
Anti-Mouse CD8β – APC	eBioscience	Clone H35-17.2; RRID:AB_657760
Anti-Mouse CD11a (LFA1) - AF647	In house	Clone FD44.8
Anti-Mouse CD16/32	In house	Clone: 24G2
Anti-Mouse CD44 – APC eF780 or Pacific Blue	eBioscience / In house	Clone IM7; RRID:AB_1272244
Anti-Mouse CD45.1 – BV 785, Pacific Blue or AF647	BioLegend / In house	Clone A20; RRID:AB_2563379
Anti-Mouse CD45.2 – PerCP Cy5.5 or BV 650	eBioscience / BioLegend	Clone 104.2; RRID:AB_953590 RRID:AB_2563065
Anti-Mouse CD45.2 – biotin	In house	Clone AL-1
Anti-Mouse CD62L – PE, PerCP-Cy5.5, BV 711 or AF647	eBioscience / BioLegend / In house	Clone Mel14; RRID:AB_465722 RRID:AB_996667 RRID:AB_2564215
Anti-Mouse CD107a (LAMP-1) – PE Cy7	Biolegend	Clone 1D4B; RRID:AB_2562146
Anti-Mouse CD122 - eF450	eBioscience	Clone TM-b1; RRID:AB_2016697
Anti-Mouse CD127 – APC or PE	eBioscience / In house	Clone A7R34; RRID:AB_469435 RRID:AB_465845
Anti-Mouse CXCR3 - PE	BioLegend	Clone 173; RRID:AB_1027656
Anti-Mouse CX3CR1 – BV 711	BioLegend	Clone SA011F11; RRID:AB_2565939
Anti-Mouse/rat Granzyme A - PE	Santa Cruz Biotechnology	Clone 3G8.5; RRID:AB_2114414
Anti-Mouse/human Granzyme B – AF647	BioLegend	Clone GB11; RRID:AB_2294995
Anti-Mouse IFN-γ - PE or PercPCy5.5	eBioscience	Clone XMG1.2; RRID:AB_466193 RRID:AB_1107020
Anti-Mouse IL-2 – APC	eBioscience	Clone JES6-5H4; RRID:AB_2535421
Anti-Mouse Ki67 – FITC	BD Biosciences	RRID:AB_396302
Anti-Mouse KLRG1 – PE Cy7 or BV 421	eBiosciences / BioLegend	Clone 2F1; RRID:AB_1518768 RRID:AB_10918627
Anti-Mouse Sca-1 - PE Cy7 or AF700	eBiosciences / BioLegend	Clone D7; RRID:AB_469669 RRID:AB_2565959

(Continued on next page)

Continued

REAGENT or RESOURCE	SOURCE	IDENTIFIER
Anti-Mouse TNFα – PE Cy7 or Pacific Blue	eBioscience / BioLegend	Clone MP6-XT22; RRID:AB_11042471 RRID:AB_893639
Anti-Mouse/human TCF1 Rabbit mAb antibody	Cell Signaling Technology	Clone C63D9; RRID:AB_2199302
Anti-Human CD8 – APC-AF750	Beckman Coulter	Clone B9.11; RRID:AB_130782
Anti-Human CD45RA – BrV510	Biolegend	Clone HI100; RRID:AB_493763
Anti-Human CD95 – PE Cy7	Biolegend	Clone DX2; RRID:AB_2100369
Anti-Human CCR7 – BrV 421	Biolegend	Clone G043H7; RRID:AB_11203894
Anti-rabbit IgG (FITC)	eBioscience	polyclonal; RRID:AB_2536525
Donkey anti-rat IgG – Cy3	Jackson Immunoresearch	Cat# 712-165-153; RRID:AB_2340667
Donkey anti-rabbit Alexa488	Life Technologies	Cat# R37118; RRID:AB_2556546
Donkey anti-rabbit IgG – Cy3	Jackson Immunoresearch	Cat# 711-165-152; RRID:AB_2307443
F(ab')2-Donkey anti-Rabbit IgG (H+L) - PE	eBioscience	RRID:AB_1210761
Goat Anti-Rabbit IgG (H+L) - AF647	Molecular Probes (Invitrogen)	RRID:AB_141663
Rabbit anti-GFP	Thermofisher	
Rat Anti-Mouse CD4	eBioscience	Clone H129
Streptavidin - APC	eBioscience	Cat# 17-4317-82
H-2D^b / gp33-41 – APC (Tetramer)	TC Metrix	N/A
H-2D^b / np396 – APC (Tetramer)	TC Metrix	N/A
H-2K^b / Ova257-264 (SIINFEKL) – APC (Tetramer)	TC Metrix	N/A
HLA-A*02 / LLW – APC (Tetramer)	TC Metrix	N/A
Bacterial and Virus Strains		
LCMV 53b Armstrong (Arm)	D. Zehn, IVR-CHUV	in house
LCMV WE	C. Mueller, Uni Bern	in house
Biological Samples		
Human blood specimens	Centre de vaccination et de médecine des voyages, Policlinique Médicale Universitaire PMU, Lausanne, Switzerland.	Study protocol 324/13 approved by the "Swiss Ethics Committee on research involving humans," Canton of Vaud, Switzerland.
Chemicals, Peptides, and Recombinant Proteins		
Ammonium-Chloride-Potassium (ACK) buffer	In house	N/A
Brefeldin A	Biolegend	Cat# 420601
DAPI	Life Technlogies	Cat# D1306
Diphtheria Toxin (DT)	Sigma-Aldrich	Cat# D0564
Dithiothreitol (DTT)	Applichem	Cat# A3668
Lipofectamine™ 2000 Transfection Reagent	ThermoFisher Scientific	Cat# 11668019
Montanide	SEPPIC, Paris, France	N/A
NP-40	Caymanchem	Cat# 600009
Pam3CSK4	InvivoGen	Cat# 112208-00-1
Peptide: LCMV glycoprotein amino acids 33-41 (gp33) (KAVYNFATM)	TC Metrix	N/A
Peptide: LCMV np396 (FQPQNGQFI)	TC Metrix	N/A

Continued

REAGENT or RESOURCE	SOURCE	IDENTIFIER
Peptide: Ovalbumin amino acids 257-264 (OVA) (SIINFEKL)	P. Romero, UNIL	N/A
Peptide: KL-SLP (KKKKKLEQLEAAYSIINFEKL)	GenScript, NJ	N/A
Percoll	GE Heathcare	Cat# 17-0891-01
Polybrene	Sigma-Aldrich	Cat# TR-1003-G
Recombinant human IL-2	Glaxo IMB, Genève, Switzerland	gift from N. Rufer
Sunflower seed oil	Sigma-Aldrich	Cat# S5007
Tamoxifen	Sigma-Aldrich	Cat# T5648
TDE1, Tagment DNA Enzyme	Illumina	Cat# 15027865
Trizol	Life Technlogies	Cat# 15596026
2xTD buffer	Illumina	Cat# 15027866
7-AAD (Viability dye)	Biolegend	Cat# 420404
Critical Commercial Assays		
Tumor Dissociation Kit	Miltenyi Biotec	Cat# 130-096-730
Mouse CD8$^+$ T cell enrichment kit	StemCell Technologies	Cat# 19853
Direct–zol RNA Mini Prep	Zymo Research	Cat# R2050
Intracellular Fix & Perm Buffer set	eBiosciences	Cat# 88-8824
FoxP3/Transcription factor staining buffer set	eBiosciences	Cat# 00-5523
SMART-Seq v4 Ultra Low Input RNA reagents	Clontech	Cat# 634888
Illumina Nextera XT DNA Library reagents	Illumina	Cat# 15032354
MACS CD8+ positive selection	Miltenyi Biotec	Cat# 130-116-478
Annexin V - APC Apoptosis Detection Kit	eBioscience	RRID:AB_2575165
SuperScript III First-Strand Synthesis System	ThermoFisher Scientific	Cat# 18080051
KAPA SYBR FAST qPCR Kit Master Mix	Kapabiosystems	Cat# KR0389
Dynabeads Mouse T-Activator CD3/CD28	ThermoFisher Scientific	Cat# 11452D
CellTrace™ Violet Cell Proliferation Kit	ThermoFisher Scientific	Cat# C34557
MinElute PCR Purification kit	QIAGEN	Cat# 28004
Illumina's Unique Dual (UD) Indexes	Illumina	Cat# 20027213
NEBNext High-Fidelity 2X PCR Master Mix	New England Biolabs	Cat# M0541
AMPure XP magnetic beads	Beckman Coulter	Cat# A63880
Zombie Aqua Fixable Viability kit	Biolegend	Cat# 423101
Deposited Data		
RNA-seq data	This study	GEO: GSE144383
ATAC-seq data	This study	GEO GSE144383
Experimental Models: Cell Lines		
Mouse: RMA		RRID:CVCL_J385
Experimental Models: Organisms/Strains		
Mouse: C57BL/6 (B6) (CD45.2)	Charles River Laboratoies	Strain 027
Mouse: B6.SJL-Ptprc < a > (B6 CD45.1)	Jackson Lab	Strain 002014; RRID:MGI:6200621
Mouse: B6; D2-Tg(TcrLCMV)327Sdz P14 T cell receptor (TCR) transgenic (CD45.2)	(Pircher et al., 1989)	RRID:MGI:3810256
Mouse: B6.129-Tm(Tcf7)Cle (*Tcf7*$^{-/-}$) (CD45.2)	Verbeek et al., 1995	RRID:MGI:4360712

(Continued on next page)

Continued

REAGENT or RESOURCE	SOURCE	IDENTIFIER
Mouse: B6.Gt(ROSA)26Sortm1 (CAG-Brainbow2.1)Cle, (CD45.2)	(Snippert et al., 2010) J. Joyce, UNIL	N/A
Mouse: B6.Tg(Tcf7^{GFP})Whe (Tcf7^{GFP}) (CD45.2)	(Utzschneider et al., 2016)	N/A
Mouse: B6.Tg(*Tcf7*$^{DTR-GFP}$)Whe (Tcf7$^{GFP-DTR}$), (CD45.2)	(Siddiqui et al., 2019).	N/A
Mouse: B6.Tg(*Tcf7*$^{CreER-GFP}$)Whe (Tcf7 $^{CreER-GFP}$), (CD45.2)	This study	N/A
Oligonucleotides		
mTcf7 Fw	Microsynth AG	TGCTGAGTGCACACTCAAGG
mTcf7 Re	Microsynth AG	TGCGGGCCAGTTCATAGTA
mArmcx2 Fw	Microsynth AG	CTGCACCCAGTCCTAAGGTTC
mArmcx2 Re	Microsynth AG	TAGCCTCAGTTTTAGCCCCAT
mElovl6 Fw	Microsynth AG	GAAAAGCAGTTCAACGAGAACG
mElovl6 Re	Microsynth AG	AGATGCCGACCACCAAAGATA
mPlxdc2 Fw	Microsynth AG	GCCGCAGCAGGAGTTATGTTA
mPlxdc2 Re	Microsynth AG	TTCATTCCAAGGAAAAGCGTTTG
mSmad1 Fw	Microsynth AG	GCTTCGTGAAGGGTTGGGG
mSmad1 Re	Microsynth AG	CGGATGAAATAGGATTGTGGGG
mKlf4 Fw	Microsynth AG	GTGCCCCGACTAACCGTTG
mKlf4 Re	Microsynth AG	GTCGTTGAACTCCTCGGTCT
mKit Fw	Microsynth AG	GCCACGTCTCAGCCATCTG
mKit Re	Microsynth AG	GTCGCCAGCTTCAACTATTAACT
mβ2 m Fw	Microsynth AG	AGACTGATACATACGCCTGCAG
mβ2 m Re	Microsynth AG	GCAGGTTCAAATGAATCTTCAG
Recombinant DNA		
pCMV-dR8.74	D. Trono, EPFL	RRID:Addgene_22036
pMD2.G	D. Trono, EPFL	RRID:Addgene_12259
pLV[shRNA]-mCherry-U6 > Scramble_shRNA	Cyagen	CCTAAGGTTAAGTCGCCCTCG
pLV[shRNA]-mCherry-U6 > mTcf7 [shRNA#1]	Cyagen	GCCACAAGTCTAAACAATAAT
pLV[shRNA]-mCherry-U6 > mTcf7 [shRNA#2]	Cyagen	TTCTCCACTCTACGAACATTT
pLV[shRNA]-mCherry-U6 > mTcf7 [shRNA#3]	Cyagen	AGAAGCCAGTCATCAAGAAAC
pLV[shRNA]-mCherry-U6 > mArmcx2 [shRNA#1]	Cyagen	CCTGGTACTGTGTCTACAAAT
pLV[shRNA]-mCherry-U6 > mArmcx2 [shRNA#3]	Cyagen	CCAGCTTTAAGCTGAACCATT
pLV[shRNA]-mCherry-U6 > mElovl6 [shRNA#1]	Cyagen	CCCATGTAGATCAAGTCATAA
pLV[shRNA]-mCherry-U6 > mElovl6 [shRNA#2]	Cyagen	GTCAGCAAATTCTGGGCTTAT
pLV[shRNA]-mCherry-U6 > mKlf4 [shRNA#1]	Cyagen	CATGTTCTAACAGCCTAAATG
pLV[shRNA]-mCherry-U6 > mKlf4 [shRNA#2]	Cyagen	AGTTGGACCCAGTATACATTC
pLV[shRNA]-mCherry-U6 > mKit[shRNA#1]	Cyagen	ACTTCGCCTGACCAGATTAAA
pLV[shRNA]-mCherry-U6 > mKit[shRNA#2]	Cyagen	CCCTGGTCATTACAGAATATT

(Continued on next page)

Continued

REAGENT or RESOURCE	SOURCE	IDENTIFIER
pLV[shRNA]-mCherry-U6 > mPlxdc2 [shRNA#1]	Cyagen	GTTCGAAGAAGAACAATTTAT
pLV[shRNA]-mCherry-U6 > mPlxdc2 [shRNA#3]	Cyagen	GTACTGGCTTACAGGTGTTAA
pLV[shRNA]-mCherry-U6 > mSmad1 [shRNA#1]	Cyagen	GGACTACCTCATGTCATTTAT
pLV[shRNA]-mCherry-U6 > mSmad1 [shRNA#2]	Cyagen	GACGAAGGAGCCACGATAATA
Software and Algorithms		
GraphPad Prism v8.0.2	http://graphpad-prism.software.informer.com/5.0/	RRID:SCR_002798
FlowJo v10	Tree Star	RRID:SCR_008520
Adobe Illustrator v24.0.1	Adobe creative cloud	https://www.adobe.com/ch_fr/creativecloud
Cutadapt (v. 1.8)	(Martin et al., 2011)	https://cutadapt.readthedocs.io/en/stable/
seq crumbs (v. 0.1.8)	http://bioinf.comav.upv.es/seq_crumbs/	N/A
STAR (v. 2.5.3a) (Dobin et al., 2013)(Dobin et al., 2013)	(Dobin et al., 2013)	https://github.com/alexdobin/STAR/releases
htseq-count (v. 0.9.1)	(Anders et al., 2015)	https://htseq.readthedocs.io/en/release_0.10.0/
RSeQC (v. 2.3.7) (Wang et al., 2012)(Wang et al., 2012)	(Wang et al., 2012)	http://rseqc.sourceforge.net/
R (v. 3.4.4 or 3..5.3).		https://www.r-project.org/
EdgeR (v. 3.20.9 or v. 3.24.3)	(Robinson et al., 2010)	https://www.bioconductor.org/packages/release/bioc/html/edgeR.html
Fastq_screen (v 0.11.1)		https://www.bioinformatics.babraham.ac.uk/projects/fastq_screen/
Reaper (v 15-065)	Davis et al., 2013	N/A
Limma (v. 3.38.3)	(Ritchie et al., 2015)	http://bioconductor.org/packages/release/bioc/html/limma.html
BiomaRt (v. 2.38.0)	(Durinck et al., 2009)	https://bioconductor.org/packages/release/bioc/html/biomaRt.html
bcbio-nextgen (v. 19.03)		https://github.com/bcbio/bcbio-nextgen
BWA (version 0.7.17-r1188)	arXiv:1303.3997v2	N/A
samtools (version 1.9)	(Li et al., 2009)	http://www.htslib.org/doc/samtools.html
Macs2 (version 2.1.1)	(Zhang et al., 2008)	https://pypi.org/project/MACS2/
DiffBind (version 2.10.0)		https://www.bioconductor.org/packages//2.10/bioc/html/DiffBind.html
CHIPpeakAnno (version 3.16.1)		https://bioconductor.org/packages/release/bioc/html/ChIPpeakAnno.html
deeptools3	(Ramírez et al., 2014)	https://deeptools.readthedocs.io/en/develop/
ComplexHeatmap (version 1.20.0)	(Gu et al., 2016)	https://bioconductor.org/packages/release/bioc/html/ComplexHeatmap.html
Integrative Genomics Viewer	(Robinson et al., 2011)	http://software.broadinstitute.org/software/igv/
Visiopharm (v. 2019.02)		https://www.visiopharm.com/
BioRender		https://biorender.com

RESOURCE AVAILABILITY

Lead Contact

Further information and requests for resources and reagents should be directed to and will be fulfilled by the Lead Contact, Werner Held (Werner.Held@unil.ch).

Materials Availability

All unique/stable reagents generated in this study are available from the Lead Contact with a completed Materials Transfer Agreement.

Data and Code Availability

The accession number for the RNA-seq and ATAC-seq data reported in this paper is GEO: GSE144383.

EXPERIMENTAL MODEL AND SUBJECT DETAILS

Mice

C57BL/6 (B6) (CD45.2) mice were obtained from Charles River (L'Arbresle Cedex, France), CD45.1 congenic B6 mice were bred locally. P14 T cell receptor (TCR) transgenic mice, expressing a TCR specific for the LCMV gp33–41 epitope (gp33) in the context of H-2D^b [P14 T cells], provided by H.P. Pircher (Freiburg, Germany) (CD45.2$^+$) (Pircher et al., 1989), *Tcf7*$^{-/-}$ mice (Verbeek et al., 1995) provided by H. Clevers (Utrecht, the Netherlands), Vβ5 TCR transgenic mice (Dillon et al., 1994) provided by P. Fink (Seattle, USA). Rosa26 lox stop lox Confetti (*R26*^{Confetti}) (Snippert et al., 2010) (provided by J. Joyce, UNIL). *Tcf7*^{GFP} (Utzschneider et al., 2016) and *Tcf7*$^{DTR-GFP}$ mice have been described (Siddiqui et al., 2019).

Tcf7$^{CreER-GFP}$ mice were generated using a bacterial artificial chromosome (BAC) containing the entire *Tcf7* locus plus > 60kb of up and down stream sequence (RP23-223A11). An EGFP-T2A-CreERT2-polyA fusion gene was inserted into the endogenous translation start codon present in exon Ia' of the *Tcf7* locus. PiggyBAC transgenic *Tcf7*$^{GFP-CreER}$ mice were generated by pronuclear injection into fertilized B6 oocytes (Cyagen Inc.). Founder mice were identified by PCR and initially characterized by flow cytometry for GFP expression.

P14 *Tcf7*^{GFP}, P14 *Tcf7*$^{-/-}$ *Tcf7*^{GFP}, P14 *Tcf7*$^{DTR-GFP}$, *Tcf7*$^{CreER-GFP}$ *R26*^{Confetti} and P14 *Tcf7*$^{CreER-GFP}$ *R26*^{Confetti} mice were obtained by breeding (all CD45.2$^+$ except indicated otherwise).

Mouse strains were maintained in the SPF animal facility of the University of Lausanne. Experiments used both male and female mice between 6 and 12 weeks of age whereby donors and recipients of adoptive T cell transfers were sex matched. Animal experiments were conducted in accordance with protocols approved by the veterinary authorities of the Canton de Vaud.

Human vaccination study

Human samples used in this study (protocol 324/13) originated from peripheral blood of n = 6 healthy volunteers (4 female and 2 male, aged 22 to 47 years) that were in the prospect of receiving the YF-17D vaccine in view of traveling to endemic areas, in collaboration with the local Centre de vaccination et de médecine des voyages (Policlinique Médicale Universitaire (PMU), Lausanne). The study protocols were approved by the "Swiss Ethics Committee on research involving humans" of the Canton of Vaud, Switzerland. All participants provided written informed consent.

METHOD DETAILS

LCMV infections

Mice were infected intraperitoneally (i.p.) with 2 × 10^5 plaque forming units (PFU) LCMV 53b Armstrong (Arm) or i.v. with 200 PFU of LCMV WE strain. For recall responses mice were infected with 2 × 10^5 PFU LCMV Arm (i.p.) (LV sh RNA experiments) or 2'000 PFU of LCMV WE (i.v.) (all other experiments).

To determine viral titers, spleens from LCMV-infected mice were 'shock frozen'. Diluted spleen suspensions were then used to infect Vero cells, and viral titers were determined by an LCMV focus-forming assay, as described elsewhere (Battegay et al., 1991). Plaque Forming Units (PFUs) were calculated per gram of spleen.

Adoptive T cell transfer

P14 CD8 T cells were obtained by mashing the spleen through a 40 μm nylon cell strainer (BD Falcon). Red blood cells were lysed with a hypotonic Ammonium-Chloride-Potassium (ACK) buffer. CD8$^+$ T cells were purified using mouse CD8$^+$ T cell enrichment kit (Stem-Cell Technologies). Purified P14 cells (CD45.2) (usually > 95% pure) were adoptively transferred intravenously (i.v.) into naive B6 (CD45.1 or CD45.1/2) one day prior to infection (d-1). For primary responses, 10^4 naive P14 cells were usually transferred. For the analyses of very early time points mice received 2x10^6 (d2 and d3) or 10^5 (d4) P14 cells. For experiments using *Tcf7*$^{-/-}$ *Tcf7*^{GFP} cells, CD62L$^+$ *Tcf7*^{GFPhi} P14 cells were sorted from the spleen of naive mice and transferred (10^4) into B6 recipient. For secondary transfer experiments involving P14 cells, B6 mice were transplanted with 10^4 flow sorted cells of the indicated phenotype. For tertiary transfers 2'000 P14 cells were injected i.v.. For transfers of polyclonal CD8$^+$ T cells, mice were transplanted with 150000 flow sorted

Tcf7^{GFP+} or 40000 *Tcf7*^{GFP-} CD8$^+$ T cells. Finally, to test the recall response of d8 LV transduced (mCherry$^+$) *Tcf7*^{GFP+} cells, 500 to 1'000 flow sorted cells were transferred. For all experiments involving flow sorted cells, cell transfer and LCMV infection and was done on the same day (d0).

Tamoxifen (TAM) and diphtheria toxin (DT) treatment

Tamoxifen (TAM) (T5648, Sigma) was dissolved in 100% ethanol to a concentration of 100 mg/mL and then diluted in pre-heated Sunflower seed oil (S5007, Sigma) to a concentration of 10 mg/mL. Mice were injected intraperitoneally (i.p) with 1mg TAM, beginning at d8 p.i. daily for 5 consecutive days.

Induction of Cre activity in *R26*^{confetti/+} cells results in the stochastic and mutually exclusive expression of one of four fluorescent proteins (RFP, CFP, YFP or GFP) (Snippert et al., 2010). Herein irreversible labeling was followed based on RFP expression, but TAM treatment also yields GFP^{hi} cells. These cells can be discriminated from *Tcf7*^{CreER-GFP+} cells based on the intermediate amounts of GFP of the latter. The GFP^{hi} cells were excluded from the analysis.

A Diphtheria Toxin (DT) (D0564, Sigma) stock solution (2 mg/mL in H$_2$O) was diluted in PBS to 5 μg/mL. Mice were injected intraperitoneally (i.p) with 50 μg/kg of body weight (around 1 μg of DT in 200 μL per mouse of 20 g). Control mice were injected with PBS

Vaccination

Tcf7^{GFP} mice were injected sub-cutaneously (s.c.) at the base of tail with a modified synthetic long Ovalbumin peptide (KKKKKLEQ-LEAAYSIINFEKL, termed KL-SLP) (15.86 nmole) (GenScript, Piscataway, New Jersey, USA) mixed with Pam3CSK4 (2 nmole) (Invivo-Gen, San Diego, California, USA) in Montanide (25 μL, SEPPIC, Paris, France)), or Pam3CSK4 only in Montanide. The immune response in the peripheral blood or spleen was analyzed using H-2K^b Ovalbumin (SIINFEKL) tetramers (K^{b}Ova) (TCMetrix) one week or 3 weeks post the boost.

Plasmids, lentiviral vectors, virus production and T cell transduction

Lentivirus U6-shRNA pgk-mCherry constructs were synthesized by Cyagen and 2nd generation packaging constructs were obtained from D. Trono (EPFL) as listed in the Key Resource Table.

For lentivirus (LV) production, 293T cells (passage number < 10) were transiently transfected with lentivirus and 2nd generation packaging plasmids (pCMV-dR8.74 and pMD2.G) using lipofectamine 2000 (ThermoFisher) in the absence of antibiotics. LV culture supernatants were collected 48 h after transfection, filtered through a 0.45μM filter (Millex) and either used directly to transduce activated CD8$^+$ T cells or stored frozen.

For T cell activation and transduction, CD8$^+$ T cells were purified from the spleen of naive P14 *Tcf7*^{DTR-GFP} mice (abbreviated here to *Tcf7*^{GFP}) as described above. The *Tcf7*^{DTR-GFP} reporter was used for these experiments since the original *Tcf7*^{GFP} reporter expresses mCherry in addition to GFP. Purified cells were activated with Dynabeads Mouse T-Activator CD3/CD28 (ThermoFisher) (in a 1:1 cells:beads ratio) in the presence of recombinant human IL-2 (50ng/mL) (a gift from N. Rufer, CHUV) *in vitro* for 24 h before the addition of viral supernatant. LV transduction of activated cells was performed in the presence of polybrene (4 μg/mL) (Sigma, TR-1003-G) during spin infection (1800rpm for 90min at 30°C). The cells were further cultured overnight at 37°C. The next morning, transduced P14 cells (10^5) were injected i.v. into mice that had been infected with LCMV Arm one day before. Alternatively, P14 cells were kept in culture for 48 h and analyzed for the transduction efficiency.

In vitro killing assay

RMA mouse tumor cells were pulsed with gp33-41 peptide (KAVYNFATM) (1μM) for 1 h at 37°C, labeled with CTV (Cell Trace Violet) (2 μM) for 8 min at 37°C and washed 3x. Gp33-pulsed RMA target cells were co-cultured with sorted *Tcf7*^{GFPhi} or *Tcf7*^{GFP-} effector cells, at the indicated effector to target cell (E:T) ratios, for 4 h at 37°C. In parallel, target cells were cultured alone to measure basal apoptosis. Following incubation, cells were stained with 7-AAD 5 min before acquisition. Target cell apoptosis was determined by the incorporation of 7-AAD among CTV$^+$ cells. The percentage of specific lysis for a given E:T ratio was calculated as 100*(%lysis-% spontaneous lysis)/(100-%spontaneous lysis), whereby spontaneous lysis corresponded to the % of apoptotic target cells in the absence of effector cells.

Tissue preparation and cell suspensions

For the analysis of Trm cells, mice were injected i.v. with 3 μg of APC-eF780-labeled anti-CD8α mAb (clone 53-6.7) 4 min prior to sacrifice. CD8α$^-$ cells were considered to be resident in non-lymphoid tissues.

For the isolation of Intraepithelial Lymphocytes (IELs) the mouse's small intestine was collected and the Peyer's patches were excise. The intestine was flushed with HBSS 2% FCS and cut in small pieces before being cut longitudinally (to open the intestine), followed by incubation with 1mM of Dithiothreitol (DTT) (Applichem, A3668) in HBSS 10% FCS and 2mM EDTA for 30min at 37°C while stirring. After digestion, the cell suspension (containing the IELs) was filtered using a 100μM strainer (Falcon) and centrifuged to obtain a pellet. The cells were then resuspended in FACS buffer and stained immediately. Alternatively, the resulting pellet was enriched for CD8 T cells using MACS positive selection (Miltenyi Biotec kit 130-116-478).

Liver and Lung were cut in small pieces and digested enzymatically with Tumor Dissociation kit (Miltenyi Biotec: 130-096-730) for 30min at 37°C. Following digestion, the tissues were further dissociated using a 40μM strainer. Hematopoietic cells were then isolated using a 40/80% discontinuous Percoll density gradient (GE Healthcare). Cells at the interface were harvested, washed 2x and red blood cells were lysed with ACK buffer.

For the analysis of bone marrow (BM) the femur was collected and flushed with RPMI 10% FCS using a 10mL syringe and a 26G needle. The BM cells were then pipeted up and down to obtain a single cell suspension and passed through a 40μM cell strainer. Finally, red blood cells were lysed using ACK buffer.

Cell suspensions from spleen and lymph nodes (LN) were obtained by mashing through a 40μM nylon cell strainer, followed by red blood cells lysis using ACK buffer.

Peripheral blood was collected into 1.5mL Eppendorf containing 15 μL of 0.5M EDTA. Peripheral blood mononuclear cells (PBMCs) were obtained by lysing the red blood cells with ACK buffer and subsequent wash with FACS buffer.

Flow cytometry and cell sorting

Surface staining was performed with mAbs for 20 min at 4°C in PBS supplemented with 2% FCS (FACS buffer) using the reagents listed in the Key Resources Table. For tetramer staining, cell suspensions were incubated with anti-CD16/32 (2.4G2) hybridoma supernatant before staining for 90min at 4°C with APC-conjugated MHC-I tetramers. Zombie Aqua Fixable Viability kit (Biolegend) was used to exclude dead cells.

For intranuclear staining, cells were surface stained before fixation and permeabilization using the Foxp3 transcription factor staining kit (eBioscience: Cat. No. 00-5523) followed by intranuclear staining in Permeabilization buffer 1x (Perm buffer).

For the detection of cytokine production, splenocytes were re-stimulated *in vitro* with LCMV gp33-41 (gp33) (1μM) or OVA$_{257-264}$ (SIINFEKL) (1μg/mL) peptide for 5 h in the presence of Brefeldin A (5μg/mL) for the last 4.5 h. Cells were stained at the surface before fixation and permeabilization (Intracellular Fixation & Permeabilization Buffer Set, eBioscience kit: Cat. No. 88-8824) followed by intracellular staining in 1x Perm buffer. For the detection of GzmA and GzmB splenocytes were cultured in the absence of peptide but in the presence of 5μg/mL of Brefeldin A for 4.5 h, before intracellular staining as described above.

To determine cytokine production by memory cell subsets, d30 *Tcf7*^{GFPhi} CD62L$^+$, *Tcf7*^{GFPhi} CD62L$^-$ or *Tcf7*$^{GFP-}$ CD62L$^-$ P14 cells (CD45.2) were flow sorted and cultured with flow sorted host splenocytes (CD45.1/.2) in the presence of LCMV gp33-41 (gp33) peptide (1μM) for 5 h, and Brefeldin A (5μg/mL) for the last 4.5 h. Intracellular staining was performed as described above.

For LAMP-1 degranulation assay splenocytes were cultured with 1 μM of gp33 peptide for 30min at 37°C, before the addition of 5μg/mL of Brefeldin A and 1μg/mL of PE-Cy7-conjugated CD107a mAb (Biolegend), followed by incubation at 37°C for 4.5 h. Mobilization of LAMP-1 was determined by the surface expression of CD107a.

For apoptosis assays splenocytes were cultured for 4 h at 37°C in the absence of growth factors. The cells were then stained using the Annexin V-APC Apoptosis Detection Kit (eBioscience), according to manufacturer instructions. 7-AAD was added 5 min prior to data acquisition.

For cell cycle analysis, flow sorted d8 *Tcf7*^{GFPhi} and *Tcf7*$^{GFP-}$ cells were fixed and permeabilized using the Foxp3 kit (eBioscience: Cat. No. 00-5523), followed by intranuclear staining with Ki67-FITC (BD Biosciences 556026) in 1x Perm Buffer. DAPI (2μg/mL) was added for the last 10min of intranuclear staining.

Cell surface stained cells were analyzed directly. Flow cytometry measurements of cells were performed on an LSR-II or Fortessa flow cytometer (BD). Data were analyzed using FlowJo (TreeStar).

For cell sorting of P14 cells, splenocytes were enriched for CD8$^+$ T cells using the mouse CD8$^+$ T cell enrichment kit (StemCell Technologies) and stained for CD45.1 (A20) or CD45.2 (clone 104). *Tcf7*^{GFPhi} and *Tcf7*$^{GFP-}$ CD45.1$^-$ CD45.2$^+$ cells were flow sorted on a FACSAria (BD) flow cytometer. The purity of sorted cells was greater than 99%, based on post-sort analysis.

Immunofluorescence labeling and microscopy

For immunohistochemistry analysis, the spleens from d8 or d30 infected mice were fixed in 1% PFA in PBS overnight, infiltrated with 30% sucrose the next day (overnight) and then embedded and frozen in OCT compound. Cryostat sections were collected on Superfrost Plus slides (Fisher Scientific), air-dried and preincubated with blocking solution containing BSA, normal mouse serum and normal donkey serum (Sigma). Then they were labeled during 1 h using the following primary reagents: Rat anti-mCD4 (H129), Mouse anti-CD45.2 biotin (AL-1) (both produced in house) and rabbit anti-GFP (Thermofisher). After washing with PBS, the following secondary reagents were applied for 1 h: Donkey anti-rat IgG Cy3 (Jackson Immunoresearch), streptavidin-APC (Biolegend) and donkey anti-rabbit IgG Alexa488 (Thermofisher). Finally, DAPI (Sigma) was used to stain the nuclei followed by mounting in DABCO (homemade). Images were acquired with a Zeiss AxioImager Z1 microscope and a AxioCam MRC5 camera.

Image analysis and cellular identification

Image quantification was performed using VIS Image Analysis software (Visiopharm, version 2019.02). Splenic tissue was detected applying a 21 pixel mean DAPI$^+$ filter, followed by smoothening the edges and filling holes of the mask using the software's functions "close" and "fill holes," respectively. Next, the mask was converted to a region of interest (ROI), annotated in gray. Within the detected total spleen ROI a similar approach was used to detect regions positive for CD4 expression, in order to identify the T cell zone (TZ), annotated in red. As the architecture of the TZ was altered in d8 spleens, this ROI was subsequently manually adjusted based on a relatively higher mean DAPI$^+$ signal, reflective of an increased nuclear density compared to the red pulp (RP). The ROI

for B cell zones (BZ) was manually drawn based on the absence of CD4 signal and relatively higher DAPI$^+$ signal density, ROI annotated in blue. ROI were manually adjusted to exclude areas with high background signal due to artifacts in any of the channels (regions annotated in white).

Nuclear identification was based on the watershed signal of the DAPI$^+$ staining. The nuclear label was expanded with 5 pixels to allow detection of both nuclear and cytoplasmic fluorescent signal. Nuclear labels exceeding the manually set threshold for CD45.2 expression, were converted to CD45.2$^+$ labeled cells. Similarly, CD45.2$^+$ labeled cells surpassing the threshold for *Tcf7* expression were labeled as *Tcf7*$^{GFP+}$ cells. Threshold settings were identical between different samples. Finally, a counting frame was applied to ensure accurate counts for all CD45.2$^-$, CD45.2$^+$ and Tcf7^{GFP+} cells within the three ROI (total spleen, TZ and BZ). The obtained counts were then used to determine the frequency of single CD45.2$^+$ cells (*Tcf7*$^{GFP-}$ P14 cells) or of double positive CD45.2$^+$ *Tcf7*$^{GFP+}$ (*Tcf7*$^{GFP+}$ P14 cells) in each zone. The frequency of cells in the RP was obtained by subtracting TZ and BZ counts from the cell counts in the total spleen ROI.

RT-qPCR analysis

For the validation of target gene silencing, *in vitro* LV-transduced P14 cells were flow sorted based on mCherry expression at 48 h post-transduction. mCherry$^+$ cells were lysed using Trizol LS (Life Technologies) and total cellular RNA was extracted using the Direct-zol RNA MiniPrep kit (Zymo Research). Next, cDNA was synthesized using the SuperScript III First-Strand Synthesis System (ThermoFisher Scientific). Real-time quantitative PCR was performed using KAPA SYBR FAST qPCR Kit Master Mix (Kapabiosystems) on a LightCycler 480 Instrument (Roche), using primers listed in the Key Resource Table. Gene expression was quantified relative to *β2 m*.

RNA-seq analysis

Flow sorted *Tcf7*^{GFPhi} CD62L$^+$ CD8$^+$ T cells from naive *Tcf7*$^{-/-}$ or WT *Tcf7*^{GFP} P14 reporter mice (CD45.2) were used to obtain cellular RNA or were adoptively transferred into B6 hosts (CD45.1/.2) that were infected with LCMV Arm. Eight or 30 days later, splenic *Tcf7*^{GFPhi} and *Tcf7*$^{GFP-}$ P14 cells were flow sorted. Sorted cells were lysed and stored in Trizol before extraction of total cellular RNA using the Direct-zol RNA MiniPrep kit (Zymo Research).

Library preparation, sequencing and data processing were performed using the methods described (Utzschneider et al., 2016). In brief, double stranded cDNA for RNA-seq library preparation was generated using SMART-Seq v4 Ultra Low Input RNA reagents (# 634888, Clontech) according to the protocol provided with the reagents beginning with 5 ng of total RNA and using 9 cycles of PCR. 150 pg of the resulting cDNA were used for library preparation with the Illumina Nextera XT DNA Library reagents (# 15032354, Illumina) using the single cell RNA-seq library preparation protocol developed for the Fluidigm C1 (Fluidigm). Cluster generation was performed with the libraries using the Illumina TruSeq SR Cluster Kit v4 reagents and sequenced on the Illumina HiSeq 2500 using TruSeq SBS Kit v4 reagents. Sequencing data were processed using the Illumina Pipeline Software version 1.82.

Purity-filtered reads were adapters and quality trimmed with Cutadapt (v. 1.3) (Martin et al., 2011) and filtered for low complexity with seq crumbs (v. 0.1.8). Reads were aligned against *Mus musculus* (version GRCm38) genome using STAR (v. 2.4.2a) (Dobin et al., 2013). The number of read counts per gene locus was summarized with htseq-count (v. 0.6.1) (Anders et al., 2015) using *M. musculus* (Ensembl v. GRCm38.82) gene annotation. Quality of the RNA-seq data alignment was assessed using RSeQC (v. 2.3.7) (Wang et al., 2012).

Differential gene expression analysis was performed using R (version 3.1.2). Genes with low counts were filtered out according to the rule of 1 count per million (cpm) in at least 1 sample, and only protein-coding genes were retained, resulting in 12138 genes analyzed. Library sizes were scaled using TMM normalization (EdgeR, v 3.8.5) (Robinson et al., 2010) and transformed to log$_2$ cpm. PCA analysis was performed on scaled log$_2$ normalized cpm of all retained genes. Differential expression was computed using the limma package for R (version 3.22.4 (Ritchie et al., 2015)) by fitting data into a linear model correcting for batch effect. Moderated t test was used for each cell population pairwise comparison and the adjusted p values were computed by the Benjamini-Hochberg (BH) method controlling for false discovery rate (FDR) independently. Genes were considered as significantly differentially expressed between any two populations of CD8$^+$ T cells at a threshold of absolute log$_2$ fold change (FC) > 1 and FDR < 0.05.

The following external gene sets were used for gene set enrichment analysis (GSEA):

1) Genes upregulated in central memory versus effector memory CD8$^+$ T cells derived from the spleen of LCMV immune mice (Tcm versus Tem cells) (GEO: GSE70813) (Mackay et al., 2016). RNA-seq data were retrieved form Gene Expression Omnibus (GEO) database (GEO: GSM1819914, GEO: GSM1819923, GEO: GSM1819915, GEO: GSM1819924) and raw counts were filtered and genes with at least 1 (cpm) in at least 1 sample were retained (n = 12566 genes). Counts were TMM-normalized and converted to log$_2$ cpm using the edgeR package (version 3.24.3) (Robinson et al., 2010) and the voom function implemented in the limma package (version 3.38.3) (Ritchie et al., 2015). Genes differentially expressed between Tcm and Tem cells were determined by fitting a linear model to the normalized gene expression data followed by empirical Bayes moderation using the functions lmFit and eBayes implemented in the limma package. P values were adjusted using the Benjamini-Hochberg procedure (Benjamini and Hochberg, 1995). In total, n = 1896 genes were significantly upregulated in Tcm compared to Tem cells. Because genes in Mackay et al. (2016) were labeled with Entrez gene IDs, we retrieved available corresponding Ensembl IDs using the biomaRt package (v. 2.38.0) (Durinck et al., 2009), resulting in n = 1737 genes used for GSEA.

2) Stem-cell-like memory signature (see Table S1 of (Pace et al., 2018)),

3) Genes upregulated in hematopoietic stem cells (M8215) (Ivanova et al., 2002),

4) Genes upregulated in adult stem cells (M1999) (Wong et al., 2008).

5) Genes upregulated in mature hematopoietic cells (M11205) (Ivanova et al., 2002).

For the last three gene sets, we retrieved gene symbols from the Molecular Signatures Database (http://software.broadinstitute.org/gsea/msigdb) (Subramanian et al., 2005) and converted human gene symbols to mouse Ensembl IDs and mouse gene symbols using the biomaRt package.

Gene set enrichment analysis was conducted similarly to the method described in (Subramanian et al., 2005), for each cell population comparison separately. All protein-coding genes detected by RNA sequencing (12138 genes) were sorted after differential gene expression analysis according to their moderated t-statistic estimate. Upregulated genes and downregulated genes were tested for enrichment separately. An enrichment score (ES) was calculated for each cell subset comparison by increasing or decreasing a running-sum statistic according to the magnitude of the t-statistic of each gene (using p = 1, see Equation 1 in (Subramanian et al., 2005). The normalized ES (NES) and associated p value were obtained by randomizing the genes included in the gene set 10^5 times. The NES was calculated by dividing the ES by the mean of the randomized ES values, and the nominal p value was equal to the proportion of randomized ES values that had a higher (for positive ES) or lower (for negative ES) value than the ES initially calculated. Each p value was then adjusted for the total number of individual ES calculated across the five gene sets and all cell population comparisons by using the Benjamini-Hochberg procedure (Benjamini and Hochberg, 1995).

We also performed a GSEA of genes differentially expressed between P14 and $Tcf7^{-/-}$ d8 $Tcf7^{GFPhi}$ cells against the hallmark gene set list (Liberzon et al., 2015). The method was the same as the one described above, except that the genes in each gene set were randomized 1000 times.

ATAC-seq analysis

ATAC-seq was performed as described (Buenrostro et al., 2015). Briefly, $5*10^4$ flow sorted CD8$^+$ T cells were washed with cold 1x PBS and resuspended in 50µL of ice-cold lysis buffer (10mM Tris-Cl (pH 7.4), 10mM NaCl, 3mM MgCl$_2$ and 0.1% (v/v) of NP-40. Cells were centrifuged immediately and the resulting pellet (nuclei) was resuspended in 50µL of transposase reaction mix (25 µL 2xTD buffer (Illumina), 2.5 µL Tn5 transposase (Illumina) and 22.5 µL of nuclease-free water), followed by incubation at 37°C for 30min (while gently shacking). Tagmented DNA was cleaned using QIAGEN MinElute PCR Purification kit as described in the kit's protocol. Library preparation was performed using Illumina's Unique Dual (UD) Indexes (R#20027213) and NEBNext High-Fidelity 2X PCR Master Mix (M0541), using the following program: 5 min 72°C, 30 s 98°C ; 10 cycles: 10 s 98°C, 30 s 63°C, 1 min 72°C: Hold: 4°C.

The libraries were then cleaned using Agencourt AMPure XP magnetic beads (A63880, Beckman). To remove both excess adaptor primers and big DNA fragments we performed double-sided magnetic bead purification. Finally, libraries were quantified using Fragment Analyzer and sequenced on an Illumina HiSeq 4000, with paired end 150 nucleotides at the Lausanne Genomic Technologies Facility.

The bcbio-nextgen pipeline (v. 19.03, https://github.com/bcbio/bcbio-nextgen) was used for initial computations of the analysis. Each sample was sequenced on 3 independent sequencing lanes, therefore the sequencing reads of each individual lane and sample were first processed separately. Reads were filtered for quality and aligned to the *Mus musculus* reference genome (mm10) using BWA (version 0.7.17-r1188) (arXiv:1303.3997v2). The three alignment files of each sample were manipulated and merged using samtools (version 1.9) (Li et al., 2009). Peak calling was performed globally for each cell population using Macs2 (version 2.1.1) (Zhang et al., 2008) with the–broad argument.

Tests of differential accessibility of chromatin among cell populations were performed in R (version 3.5.3) using package DiffBind (version 2.10.0). Chromatin regions were considered as significantly differentially accessible between any two cell populations at a threshold of FDR < 0.05.

Principal component analysis was performed using reads per kilobase per million mapped reads (RPKM) of all accessible regions called by Macs2 (n = 112069). Subsequently, accessible chromatin regions were annotated to genes using the R package CHIPpeakAnno (version 3.16.1) and its precompiled Ensembl mouse TSS annotation (TSS.mouse.GRCm38), retaining only regions laying within ± 5kb of a gene for subsequent analyses. Heatmaps of read coverage per region were generated using the computeMatrix function of the Galaxy instance of deeptools3 (Ramírez et al., 2014). Regions smaller than 4kb were extended 2kb up- or downstream of the peak center. Read coverage per chromatin region was averaged over the 3 biological replicates of each cell population, and heatmaps were drawn using the ComplexHeatmap package (version 1.20.0) (Gu et al., 2016).

Figures of coverage tracks were exported from bigwig read alignment files using the Integrative Genomics Viewer (Robinson et al., 2011). The same y axis scale was set across all samples.

Human peripheral blood collection and analysis

Peripheral blood mononuclear cells (PBMC) were obtained from heparinated whole blood diluted 1:1 in PBS, and subjected to density gradient fractionation using Lymphoprep (30 min at 400 g without break). PBMC were cryopreserved in complete RPMI 1640 supplemented with 40% FCS containing 10% DMSO (dimethyl sulfoxide).

Frozen PBMC were thawed in RMPI containing 10 ug/mL of DNase I (Sigma), resuspended in FACS buffer (PBS 5mM EDTA, 0.2% BSA and 0.2% sodium azide) and subjected to CD8$^+$ T cell enrichment (Negative enrichment kit from Stem Cell). Cells were then stained in the following order: 1) A2/LLW tetramer (30 min at 4°C in FACS buffer) followed by a wash in FACS buffer, 2) surface staining

(in FACS buffer) followed by a PBS wash 3) staining with fixable viability dye in PBS followed by a PBS wash, 4) cells were then fixed overnight at 4°C and washed in permeabilization buffer (Foxp3 staining kit from eBioscience) 5) rabbit anti-TCF1 staining in permeabilization buffer followed by secondary fluorochrome-conjugated anti-rabbit IgG at 4°C. Specific TCF1 staining was further ascertained using a secondary antibody-only control. The cells were resuspended in FACS buffer for sample acquisition using an LSRII flow cytometer (Beckton Dickinson). Data files were analyzed using FlowJo 9.7.7.

The majority of the PBMC samples in this study (n = 5 from protocol 324/13) were stained for TCF1 using a secondary anti-rabbit FITC Ab (bioRxiv 808774). One sample was stained with secondary anti-rabbit PE Ab (shown in Figure 5I), accounting for the improved discrimination of TCF1^{hi} and TCF1^{lo} cells. Regardless of the secondary Ab used, gating of A2/LLW tetramer$^+$ TCF1^{hi} cells was based on the TCF1 staining of total naive and total CCR7$^-$ CD8$^+$ T cells present in the same sample.

QUANTIFICATION AND STATISTICAL ANALYSIS

The fold expansion of T cells was appraised relative to an estimated 10% "take" of the transferred cells (Blattman et al., 2002).

All bar and line graphs depict means ± SD. Statistical analyses were performed using Prism 7.0 or 8.0 (Graphpad Software). Non-paired t test (two-tailed, 95% confidence level) was used for the comparison of 2 datasets. One-way or two-way analysis of variance (ANOVA) was used for > 2 comparison groups. Statistical details of each experiment can be found in the figure legends. p values (p) <0.05 were considered significant (*: $p < 0.05$; **: $p < 0.01$; ***: $p < 0.001$; ****: $p < 0.0001$); $p > 0.05$ was considered non-significant (ns).